2017

Liposome-coated Magnesium Phosphate Nanoparticle for Delivery of Cytochrome C into Lung Cancer Cells A549

Weizhou Yue
University of the Pacific, w_yue@u.pacific.edu

LIPOSOME-COATED MAGNESIUM PHOSPHATE NANOPARTICLE FOR DELIVERY OF CYTOCHROME C INTO LUNG CANCER CELLS A549

by

Weizhou Yue

A Thesis Submitted to the

Office of Research and Graduate Studies

In Partial Fulfillment of the

Requirements for the Degree of

MASTER OF SCIENCE

Thomas J. Long School of Pharmacy and Health Sciences
Pharmaceutical and Chemical Sciences

University of the Pacific
Stockton, CA

2017

LIPOSOME-COATED MAGNESIUM PHOSPHATE NANOPARTICLE FOR DELIVERY OF CYTOCHROME C INTO LUNG CANCER CELLS A549

by

Weizhou Yue

APPROVED BY:

Thesis Advisor: Xin Guo, Ph.D.

Committee Member: Xiaoling Li, Ph.D.

Committee Member: John C. Livesey, Ph.D.

Department Chair: William K. Chan, Pharm.D., Ph.D.

Dean of Graduate School: Thomas H. Naehr, Ph.D.

LIPOSOME-COATED MAGNESIUM PHOSPHATE NANOPARTICLE FOR DELIVERY OF CYTOCHROME C INTO LUNG CANCER CELLS A549

Weizhou Yue

DEDICATION

This thesis is dedicated to my parents for their love and support, and is also dedicated to my beloved grandmother.

ACKNOWLEDGMENTS

My appreciation goes to Dr. Xin Guo who patiently guides me like teacher, like father. His generosity, kindness, and optimism affect me a lot and gradually lead me to become a real scientist. I also express my gratitude to Dr. Xiaoling Li who took me to University of the Pacific and gave a chance to study here and enjoy the life here. I sincerely thank my committee member Dr. John C. Livesey as well, for his precious time and respected contribution to my thesis research. My deepest thanks will be given to my labmates especially Yifan(Bob), Shen, Yingbo, Mallika and Harsha. I would like to extend my thanks to all faculty, staff and schoolmates I have met at University of the Pacific.

Liposome-coated Magnesium Phosphate Nanoparticle for Delivery of Cytochrome C into Lung Cancer Cells A549

Abstract

by Weizhou Yue

University of the Pacific
2017

Proteins are large biomolecules that have great therapeutic potential in treating many human diseases. However, chemical/enzymatic degradation, denaturation, and poor penetration into cells are some of the challenges for clinical use of intracellular proteins.

Previously, our group has developed cationic lipid-coated magnesium phosphate nanoparticle (LP MgP NP-CAT) formulations to enhance the intracellular delivery of the negatively charged protein catalase. The goal of the current research is to develop a formulation to deliver cytochrome c (CytC), a positively charged protein into lung cancer cells A549. Specifically, this thesis research prepares and tests liposome-coated magnesium phosphate nanoparticle for delivery of cytochrome c (CytC LP/MgP).

CytC LP/MgP was designed, prepared and characterized, showing that it had an average diameter around 150 nm and ζ-potential around +30 mV. The morphology of CytC LP/MgP was validated by transmission electron microscopy.

CytC LP/MgP successfully led to the attachment of CytC to A549 cells, as supported by fluorescence imaging. Intracellular delivery of CytC alleviated the cytotoxicity of cationic lipids in A549 cells, as suggested by the MTS assay on cell viability, which could facilitate the clinical use of cationic lipids in drug delivery systems.

TABLE OF CONTENTS

LIST OF TABLES

Table Page

LIST OF FIGURES

Figure Page

LIST OF ABBREVIATIONS

cDNA	complementary DNA
arg	arginine
his	histidine
pro	proline
ser	serine
PLC-γ1	phospholipase C-γ1
AT_1	angiotensin II receptor type 1
c-src	proto-oncogene tyrosine-protein kinase Src
RASM	rat aortic smooth muscle
CytC	cytochrome c
ABTS	2,2’-azino-bis(3-ethylbenzthiazoline-6-sulfonate)
MSN	mesoporous silica nanoparticle
CPPs	cell penetrating peptides
TFA-DODAPL	trifluoroacetylated lipopolyamine
DOPE	dioleoyl phosphatidylethanolamine
NP	nanoparticles
GFP	green fluorescent protein
$\Delta\Psi_m$	inner transmembrane potential

APOA-I	apolipoprotein A-I
Cre	Cre recombinase
Cas9	CRISPR associated protein 9
sgRNA	single-guide RNA
CaP	calcium phosphate nanoparticles
MgP	magnesium phosphate nanoparticles
LP/MgP	cationic liposome-coated magnesium phosphate nanoparticles
FDA	Food and Drug Administration
ROS	reactive oxygen species
CytC LP/MgP	cationic liposome-coated magnesium phosphate nanoparticles containing cytochrome c
DOTAP	1,2-dioleoyl-3-trimethylammonium-propane
C_{18}	18 carbon atoms
MOMPP	mitochondrial outer membrane permeabilization pore
ETC	electron transport chain
Apaf-1	apoptotic protease-activating factor 1
dATP	deoxyadenosine triphosphate
CytC LP	cytochrome c-encapsulated cationic liposomes
PFA	paraformaldehyde
NIH	National Institutes of Health
FBS	fetal bovine serum
NRK	normal rat kidney

HEPES	4-(2-hydroxyethyl)-1-piperazineethanesulfonic acid
TEM	transmission electron microscope
DLS	dynamic light scattering
NSCLC	non-small cell lung cancer
MTS	3-(4,5-dimethylthiazol-2-yl)-5-(3-carboxymethoxyphenyl)-2-(4-sulfophenyl)-2H-tetrazolium
DMEM/F-12	Dulbecco's modified eagle medium: nutrient mixture F-12
NHS ester	succinimidyl ester
DMSO	dimethyl sulfoxide
Alexa 488-labeled CytC	Alexa Fluor® 488-labeled cytochrome c
Alexa 488-labeled CytC LP	Alexa Fluor® 488-labeled cytochrome c-encapsulated liposomes
Alexa 488-labeled CytC LP/MgP	Alexa Fluor® 488-labeled cytochrome c-encapsulated liposomes with MgP nanoparticles
Alexa 488-labeled CytC+MgP	Alexa Fluor® 488-labeled cytochrome c-complexed with MgP nanoparticles
bare LP	bare DOTAP/cholesterol liposomes
bare LP/MgP	bare DOTAP/cholesterol liposomes with MgP nanoparticles
PBS	phosphate-buffered saline

Chapter 1: Current Development of Devices for Intracellular Protein Delivery

1.1 Introduction

Proteins represent the most diverse molecules in biology. In the past thirty years, proteins purified from natural sources or produced from recombinant biotechnology have found a plethora of applications in modern medicine, including supplementation or modulation of a biological function, targeting specific cell types, vaccination, and diagnostics [1]. Up till now, more than a hundred proteins have been approved by FDA as therapeutic or diagnostic agents in USA. Compared to small molecule drugs, proteins as therapeutics agents carry the potential advantages of exerting more complicated activities, higher specificity, higher bio-compatibility and, in average, shorter time for drug development/approval [1]. With accelerated understanding of the cellular functions of proteins after the completion of the human genome project, the role of proteins in modern medicine is expected to expand remarkably in the next decade [1].

Nevertheless, one common challenge of developing protein-based medications is to achieve an adequate pharmacokinetic profile, including long enough half-life in blood circulation and sufficient distribution to the target site [2]. After administration, native proteins are prone to enzymatic degradation and hepatic/renal elimination while circulating in the blood, and are too large to diffuse into cells. Therefore, the development of technologies to enhance the delivery of proteins to their target site is critical for capitalizing on their potential as future therapeutic agents.

In this chapter, the current development of devices for intracellular protein delivery is reviewed and summarized.

1.2 Microinjection

Single-cell microinjection has been successfully used to deliver exogenous proteins, cDNA constructs, peptides, drugs and particles into transfection-challenged cells through a glass micropipette. Due to its advantage of precise control over dosage and timing, microinjection has been widely used in studies on primary cultured cells, transgenic animal production, *in vitro* fertilization and RNA interference.

The p53 tumor suppressor is a transcription factor frequently mutated in human malignancies. Tumor-derived p53 missense mutants are defective in sequence-specific DNA binding and fail to activate p53 target genes, Abarzua *et al.* showed that microinjection of mAb PAb421, which was shown previously to restore DNA binding to selected p53 mutants *in vitro*, restored the transcription activation function of the resident mutant p53 in human SW480 colorectal carcinoma cells (arg to his 273, pro to ser 309) [3]. The results supported the concept of restoring wild-type function to mutant p53 as a strategy for cancer therapy.

1.3 Electroporation

Electroporation applies an electric current across a cell membrane to perform temporary “pores” formation, which allow exogenous molecules in the medium to enter either the cytoplasm or the nucleus, thereby transfecting or transforming the cell.

In vascular smooth muscle cells, rapid tyrosine phosphorylation of phospholipase C-γ1 (PLC-γ1) is the mechanism of how the binding of angiotensin II occupancy of the angiotensin II receptor AT^1 mobilizes calcium from the cytoplasm to eventually cause the

contraction of the smooth muscle cell. Marrero *et al.* reported that intracellular delivery of $pp60^{c\text{-}src}$ antibodies inhibited the angiotensin II phosphorylation of PLC-γ1 in cultured rat aortic smooth muscle (RASM) cells [4]. These data provided the first evidence for a direct involvement of $pp60^{c\text{-}src}$ kinase in angiotensin II-mediated PLC-γ1 phosphorylation.

1.4 Mesoporous Silica Nanoparticles

Mesoporous silica nanoparticles with high surface areas (>800 m^2/g) and tunable pore diameter (2-10 nm) were synthesized to develop a variety of new delivery formulations, where different guest molecules, such as small molecular drugs, fluorescent imaging agents, and proteins, could be absorbed into the mesopores and released into solutions later.

It is known that cytochrome c (CytC) catalyzes the oxidation of 2,2'-azino-bis(3-ethylbenzthiazoline-6-sulfonate) (ABTS) by hydrogen peroxide. Slowing *et al.* found that MCM-41-type mesoporous silica nanoparticle (MSN) with a large average pore diameter (5.4 nm) could serve as a transmembrane delivery vehicle for controlled release of the protein CytC in live human cervical cancer cells (HeLa), which find many important pharmaceutical applications as therapeutics and diagnostic agents [5].

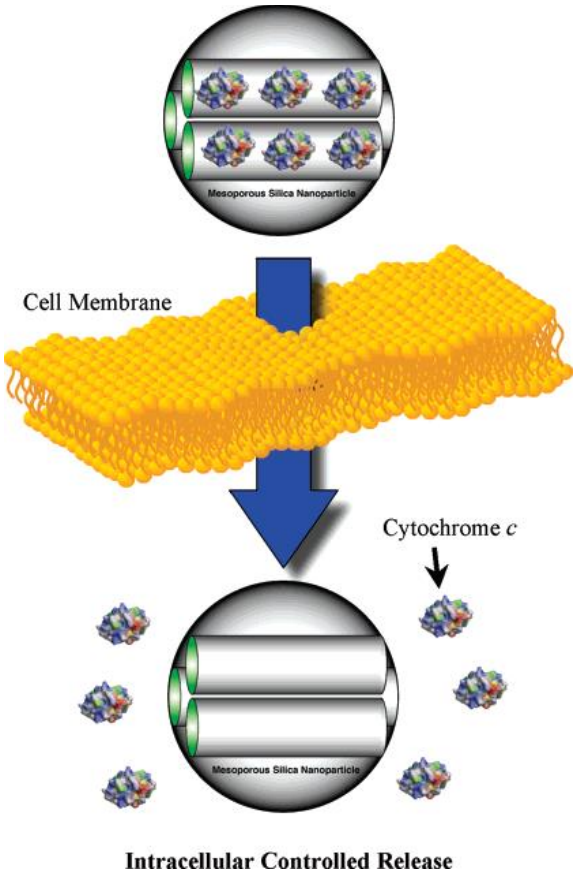

Fig. 1.1. Schematic representation of the MSN transporting cytochrome c through the cell membrane and releasing the protein into the cytoplasm [5].

1.5 Cell Penetrating Peptides (CPPs)

Short peptides isolated from protein-transduction domains (cell penetrating peptides or CPPs) of various protein types allow the intracellular delivery of conjugated (or fused) biomolecules. A wide range of cargos such as antigenic peptides, peptide nucleic acids, antisense oligonucleotides, full-length proteins, or even nanoparticles and liposomes have been intracellularly delivered by this way.

Räägel *et al.* presented the characterization of intracellular trafficking of 3 different CPP–avidin complexes (transportan-, nona-arginine- and Tat-avidin) in Cos-7

cells related to different endocytic routes during CPP-cargo internalization, which proved characteristic properties of CPPs chose pathways to gain entry to cells [6].

1.6 Cationic Liposomes

Liposomes are artificial vesicles composed essentially of mostly phospholipids and have been reported to serve as immunological adjuvants and drugs carriers. Furthermore, cationic liposomes are currently used as non-viral delivery systems, because DNA or proteins that are negatively charged readily form a complex with cationic liposomes via electrostatic interactions.

1.6.1 The Delivery System Composed of TFA-DODAPL and DOPE

Zelphati *et al.* reported a cationic liposomal formulation composed of a new trifluoroacetylated lipopolyamine (TFA-DODAPL) and dioleoyl phosphatidylethanolamine (DOPE), successfully delivered antibodies, dextran sulfates, phycobiliproteins, albumin, and enzymes (β-galactosidase and proteases) into the cytoplasm of numerous adherent and suspension cells [7]. This advanced protein delivery system represented a powerful tool for functional protein delivery and might have potential for therapeutic applications.

1.6.2 Nanoparticle Composed of DOTAP/DOPE and APOA-I

Amphiphilic residues, such as cell penetrating peptides (CPPs), have been conjugated to non-lipophilic proteins such as CytC and GFP to anchor the proteins into the lipid bilayer of nanoparticles (NP). For example, Kim *et al.* reported that a NP composed of lipid (DOTAP/DOPE) and apolipoprotein (APOA-I) delivered intracellularly-acting proteins (*e.g.* CytC or GFP) into non-small cell lung tumors. This

nanoparticle holds great potential for the effective delivery of non-lipophilic proteins for cancer therapy [8].

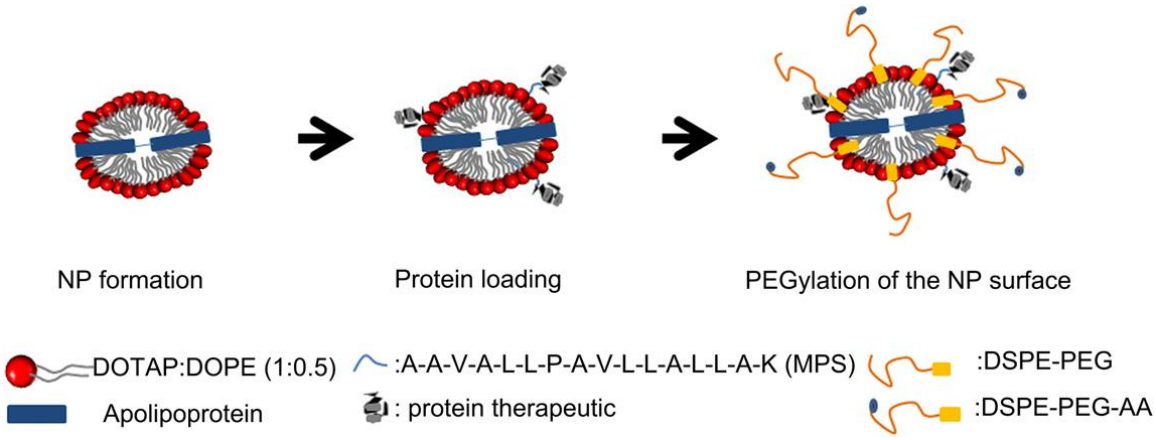

Fig. 1.2. Schematic representation of nanoparticle preparation for protein delivery [8].

1.6.3 Commercially Available Cationic Lipids

Zuris *et al.* reported that cationic lipids that are commonly used as nucleic acid transfection reagents could potently deliver proteins that were fused to negatively supercharged molecules (*e.g.* (-30)GFP-Cre, Cas9:sgRNA complexes) [9]. These findings suggested that the intracellular delivery of polyanionic proteins and protein:nucleic acid complexes by cationic lipids might expand the research and therapeutic applications of proteins.

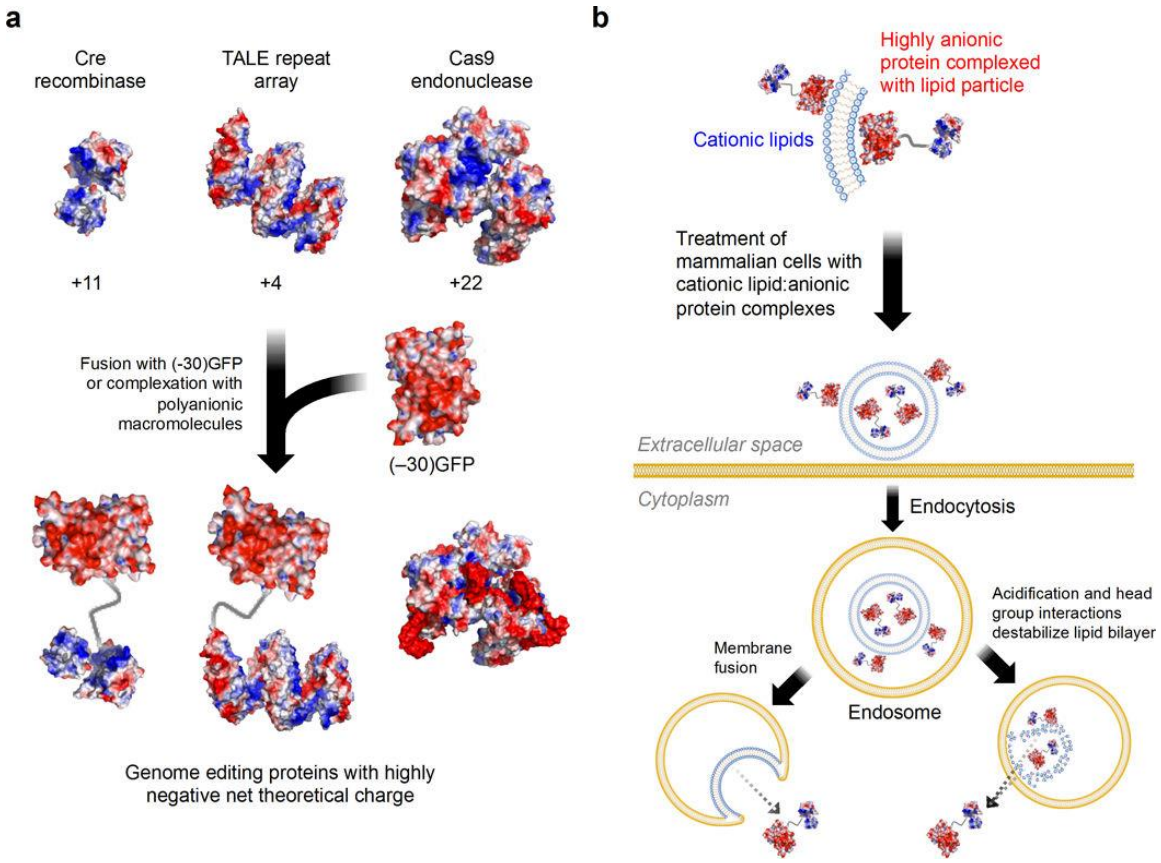

Fig. 1.3. Strategy for delivering proteins into mammalian cells by fusion or non-covalent complexation with polyanionic macromolecules and complexation with cationic lipids [9].

1.6.4 Cationic Liposome Coated-Magnesium Phosphate Nanoparticles (LP/MgP)

The low efficiency of endosomal escape and the high level of lysosomal degradation are major challenges to all protein delivery systems that enter the cells via endocytosis. Our group previously developed liposome-coated magnesium phosphate nanoparticle (LP MgP NP-CAT), which is designed to destabilize the endosome and release the cargo at lowerd pH, loaded with negatively charged protein that degrades hydrogen peroxide in cells. Intratracheal administration of LP MgP NP-CAT loaded with catalase that significantly lowered ROS levels in mouse lungs, demonstrating its great promise for protein-based therapy in the clinic [10].

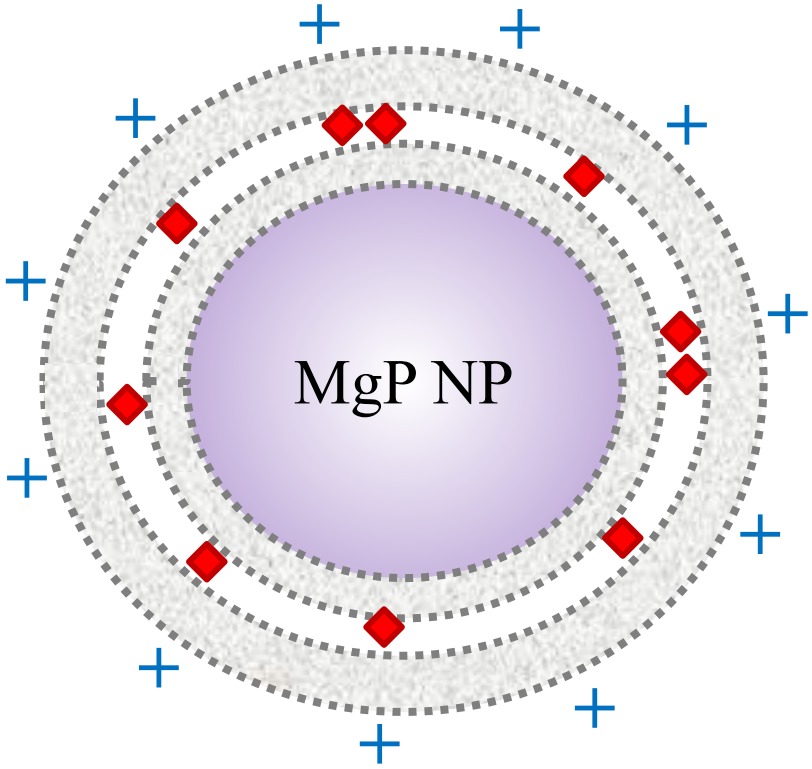

Fig. 1.4. Schematic image representing the LP/MgP for protein delivery [10]. +: Positive charges of LP/MgP; MgP NP: magnesium phosphate nanoparticles (MgP); red squares: cargo proteins; and gray circles: lipid membranes (LP) consisting of DOTAP/cholesterol.

1.7 Conclusion

Although the abovementioned delivery devices display their great promises for therapeutic applications, their drawbacks are also noticeable. Microinjection and electroporation require specialized equipment and technical skill to prevent cell damage and is not convenient when a large number of cells need to be assessed simultaneously for intercellular trafficking; cell penetrating peptides (CPPs) generate too many unwanted side effects due to their unintended penetration to untargeted normal cells; nanoparticles including mesoporous silica nanoparticles with large pores and commercially available

cationic liposomes generally suffer from low tolerance of serum, poor endosomal escape, and limited *in vivo* efficacy [9]. Therefore, novel protein delivery systems that could minimize these drawbacks would lead the advances of protein-based pharmacotherapy.

Table 1.1. Reported intracellular protein delivery systems.

Approaches	vehicles	Cargoes	Drawbacks
Microinjection		mAb PAb421	Require specialized equipment and expertise to prevent cell damage; inconvenient for delivering to a large number of cells
Electroporation		pp60c-src antibodies	Highly disruptive, cytotoxic, and inefficient
Nanoparticles	Mesoporous Silica Nanoparticles with large pores	cytochrome c	Physicochemical properties limit *in vivo* application
Cell-penetrating peptides (CPPs)	Transportan	avidin	Excessive side effects
	Oligoarginine		
	Tat		
Liposomes	A trifluoroacetylated lipopolyamine (TFA-DODAPL) and dioleoyl phosphatidylethanolamine (DOPE)	antibodies, dextran sulfates, phycobiliproteins, albumin, and enzymes (β-galactosidase and proteases)	Degradation in serum, poor endosomal escape, limited *in vivo* efficacy
	A nanoparticle (NP) composed of lipid (DOTAP/DOPE) and apolipoprotein (APOA-I)	intracellular-acting protein drugs (GFP, cytochrome c)	Poor endosomal escape
	Commercially available cationic lipids	negatively supercharged proteins ((−30)GFP-Cre, Cas9:sgRNA complexes)	Degradation in serum, poor endosomal escape, limited in vivo efficacy

Chapter 2: Design of Magnesium Phosphate Nanoparticles with Cationic Lipid Coating for Intracellular Delivery of Cytochrome C (CytC LP/MgP)

2.1 Introduction

Current non-viral vectors possess several potential advantages, such as ease of large-scale production, the capacity to carry large cargos as well as the potential to exhibit relatively lower immunogenicity in comparison to viral approaches. However, non-viral vectors typically exhibit relatively lower delivery efficiencies when compared to viral approaches. For non-viral vectors, lower delivery efficiencies (in comparison to viral approaches) were observed because of entrapment in endosome/lysosome, degradation, and inefficient cellular uptake. To solve these problems, Olton *et al.* developed a formulation of CaP nanoparticles with cationic lipid-coating because of CaP's biodegradability, biocompatibility, and ease of handling. CaP increased the fraction of the cargo that both successfully escaped from endosomes and effectively trafficked to the cytosol. The cationic lipid-coating of the formulation also helped to protect the cargo from denaturation [11].

Inspired by this design, our group recently developed a novel delivery system-magnesium phosphate nanoparticle coated with cationic lipid (LP/MgP) for intracellular protein delivery. Protein cargos were chosen because protein therapeutics have high specificity in action, and innate proteins for therapy are well tolerated and less likely to elicit immune responses. Therapeutic protein cargos also enjoy faster clinical development and shorter FDA approval time than small-molecule drugs. Moreover,

protein therapeutics are easier to obtain extensive patent protection. Negatively charged protein catalase was complexed with cationic liposome-coated magnesium phosphate nanoparticles by electrostatic interaction. The formulation reduced ROS level by 60% in EA.hy926 cells [10].

Based on the foregoing, the hypothesis of this thesis project is that liposome-coated magnesium phosphate nanoparticles (LP/MgP) can also enhance the intracellular delivery of positively charged proteins such as cytochrome c (CytC). CytC can be complexed non-specifically and delivered by rehydrated lipids *in vitro*, where this protein-liposome complexation is dependent on high protein concentrations.

This thesis research proposes to formulate liposome-coated magnesium phosphate nanoparticles containing the positively charged cargo protein, cytochrome c (CytC LP/MgP). Such CytC LP/MgP formulation comprises a core of MgP, a coating of cationic lipids, and the encapsulated cargo protein cytochrome c.

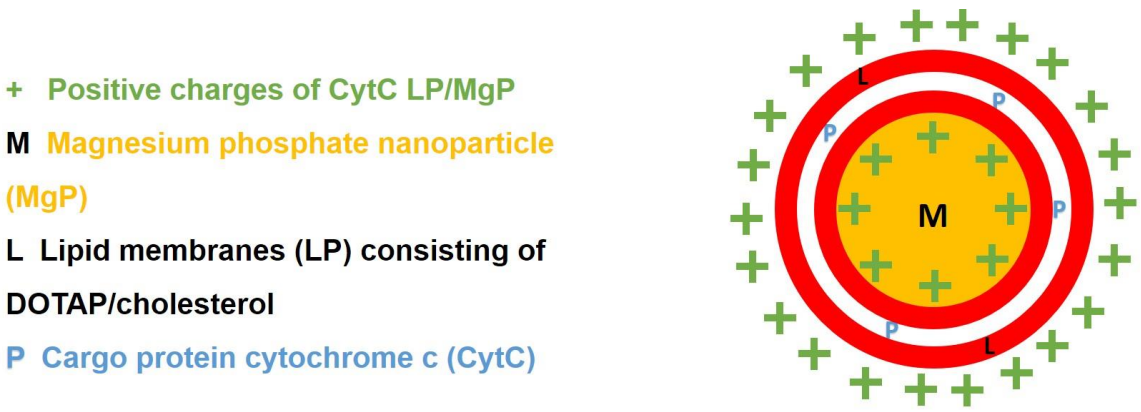

Fig. 2.1. Diagram of CytC LP/MgP.

2.1.1 Lipid – DOTAP

Kawakami *et al.* demonstrated that cationic liposomes composed of DOTAP/cholesterol accumulated in the lung one minute after intravenous injection [12]. Cationic liposomes are internalized by endocytosis in these cells. Notably, fusion of liposomes with the endosomal membrane during endosome maturation can facilitate the endosomal escape of cationic lipid-delivered cargo [13]. Furthermore, C_{18} unsaturated hydrophobic chains of cationic lipid DOTAP allow DOTAP/cholesterol liposomes to be extruded through the 100-nm polycarbonate membrane readily at room temperature. Last but not least, cationic lipids are often mixed with so-called helper lipids, such as dioleoyl phosphatidylethanolamine (DOPE) or cholesterol. The helper lipids would enhance the lipid transition from the lamellar phase to a non-lamellar structure, which would improve the delivery efficiency [14].

However, high cytotoxicity was observed in a concentration-dependent manner for DOTAP/cholesterol liposomes. It is well-known that the cytotoxicity of cationic liposomes is due to apoptosis. Mechanisms of toxicity by cationic liposomes include change of mitochondrial membrane potential, generation of reactive oxygen species (ROS), dissociation of cytochrome c from the inner mitochondrial membrane, formation of the mitochondrial outer membrane permeabilization pore (MOMPP), release of cytochrome c, and apoptosis [15]. Therefore, alleviating the toxicity of cationic liposomes becomes an important issue for the development of liposomal delivery systems.

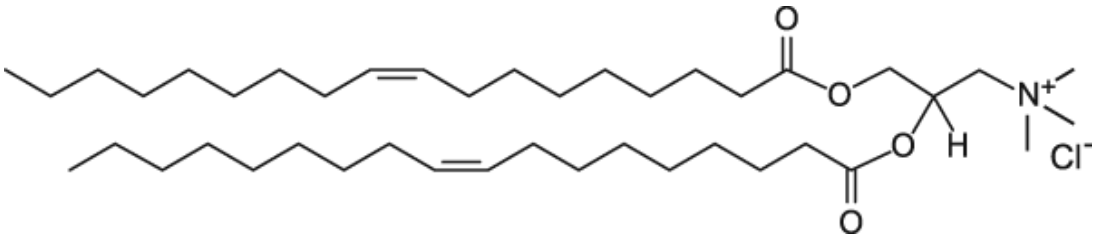

Fig. 2.2. Chemical structure of DOTAP, a commonly used cationic lipid [15].

2.1.2 Magnesium Phosphate Nanoparticle (MgP) as the Core of the Proposed Formulation

Calcium phosphate precipitation has been one of the most common techniques to transfect cultured cells in biological research. Roy *et al.* reported that after calcium chloride and sodium phosphate solutions were each dispersed into organic solvents to form two separate water-in-oil microemulsions, calcium phosphate precipitates at 100-120 nm in diameter were reliably generated by mixing two emulsions at low temperature [16]. Later, Li *et al.* reported that when calcium phosphate precipitates were coated with sodium citrate, excessive negative surface charges prevented their aggregation. Moreover, when such negatively charged calcium phosphate precipitates were mixed with cationic liposomes consisting of DOTAP/cholesterol, the cationic liposomes spontaneously wrapped around the calcium phosphate precipitates by electrostatic interaction to form calcium phosphate nano-precipitates that are coated by concentric lipid membranes [17].

One remarkable property of these nano-precipitates is that they promptly dissolve when the pH decreases from 8 to 5. Therefore, calcium phosphate precipitates are expected to dissolve and turn into a highly concentrated calcium phosphate solution after their endocytosis, when they are exposed to the acidic endosomal pH. The solution

would then absorb water because of its high osmotic pressure, swell to destabilize the endosome membrane, and release the cargo into the cytosol, thus greatly enhancing the delivery efficiency.

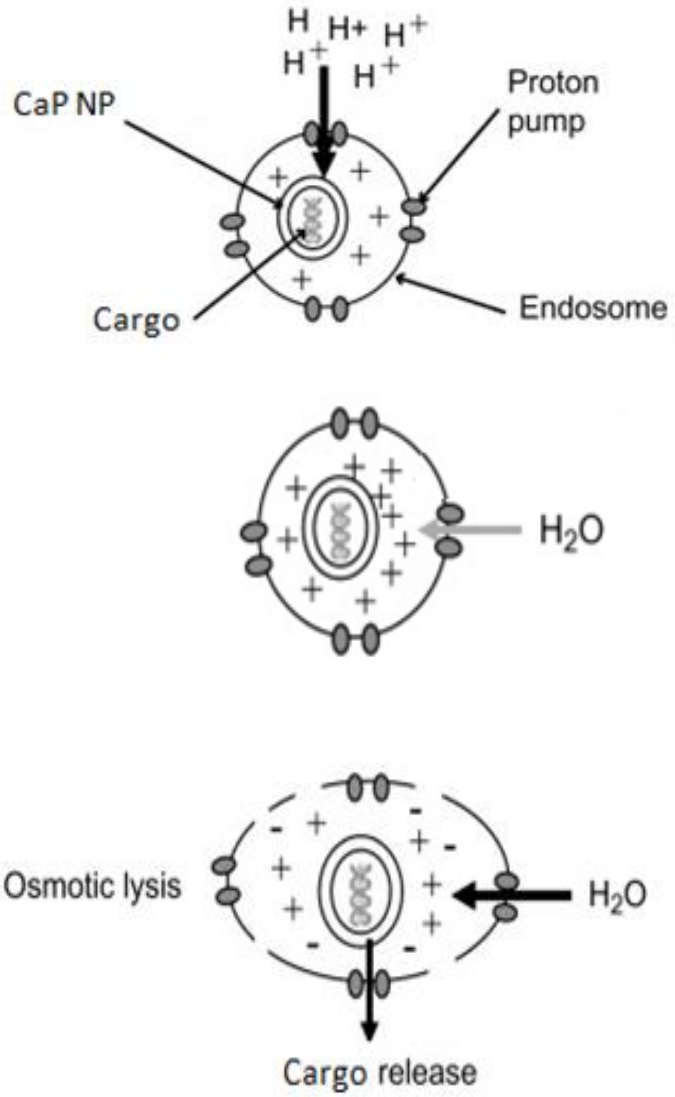

Fig. 2.3. The hypothesized release process of cargos that are entrapped in liposome-coated calcium phosphate nano-precipitates in endosomes [17].

Under physiological conditions, the extracellular Ca^{2+} concentration is ~1.2 mM whereas the cytosolic concentration is ~0.1 μM. Low to moderate elevation of the Ca^{2+} concentration (0.2~0.4 μM) in the cytosol triggers apoptosis and higher cytosolic concentrations of Ca^{2+} (>1 μM) are associated with necrosis [18]. Therefore, it is beneficial to use magnesium phosphate precipitates (MgP) as the core of the proposed formulation instead of calcium phosphate to achieve lower cytotoxicity.

2.1.3 Cargo Protein Cytochrome C (CytC)

Cytochrome c (CytC) is a small hemeprotein found loosely associated with the inner membrane of mitochondria, and is a member of the family of cytochromes. Unlike other cytochromes, CytC is highly water-soluble. It is an essential component of the electron transport chain (ETC) with isoelectric point (pI) values in the range of 10.0-10.5, therefore carrying excessive positive charges at pH 7.4.

Interestingly, it has long been known that isolated mitochondria can reversibly release and take up CytC, while the latter restores mitochondrial function [19]. Piel *et al.* reported an interesting and medically important example for the reversibility of CytC release, where intravenously injected CytC was taken into the cardiomyocytes and significantly improved the mitochondrial function in an animal model of sepsis. The survival rate increased from 15% for the controls to about 50% in the septic mice that received the CytC injections [20], [21].

CytC is also known as a mediator of apoptosis through the intrinsic apoptosis pathway. CytC is released from mitochondria into the cytosol due to formation of mitochondrial outer membrane permeabilization pore (MOMPP) when cells are stressed, and binds with apoptotic protease-activating factor 1 (Apaf-1). The binding in turn

induced the binding between the CytC/Apaf-1 complex and dATP, which is necessary for oligomerization and formation of the apoptosome. The apoptosome then recruits multiple procaspase-9 molecules and promotes their cleavage and activation into what are known as initiators of apoptosis. Caspase-9 bound to the apoptosome acts as the cleavage factor of caspase-3, which is considered as the major enzyme that initiates the degradation of numerous cellular proteins to complete the apoptosis process [22].

Although CytC release is an essential step in the apoptotic cascade but that CytC release is not sufficient to induce death in all cells. CytC-induced apoptosis is dependent on the concentration of cytosolic CytC, in that the release of endogenous CytC occurs proportionally to the extent of cellular ‘stress’ and that a certain threshold of released CytC must be reached before a cell commits to apoptosis [23].

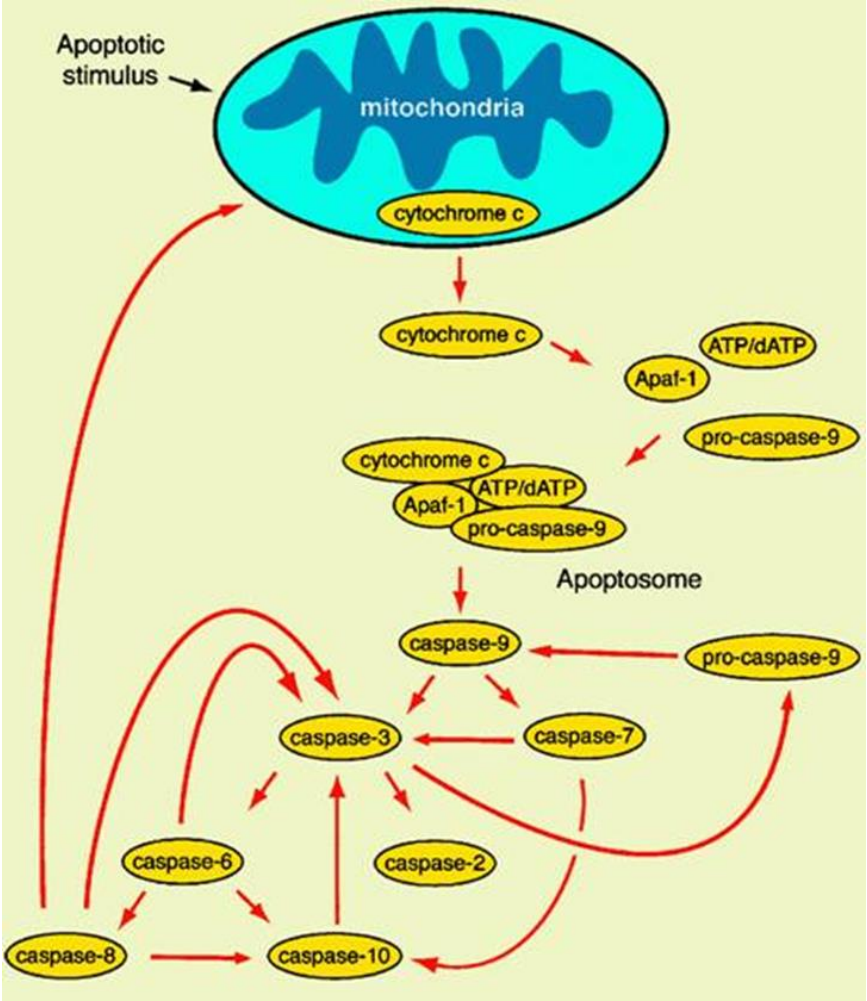

Fig. 2.4. Apoptosis pathways that involve cytochrome c (CytC) [22].

Free CytC also functions as a radical scavenger within the inner-membrane space. The oxidized form of CytC neutralizes superoxide, while both reduced and oxidized states of CytC deactivate hydrogen peroxide. Since CytC constantly undergoes oxidation/reduction cycles in a respiring cell, both detoxification reactions can take place in the mitochondria by cytochrome c as a strong antioxidant [22].

2.2 Proposed Mechanism of Protein Delivery by the Proposed CytC LP/MgP

At pH 7.4, the delivery system is expected to protect the cargo protein and to interact with the target cells either by ionic interactions. After endocytosis, the elevated

concentration of protons inside the endosome will dissolve the MgP nano-core, which will then absorb water, expand in volume, and destabilize the endosomal membrane to release the cargo protein into cytosol.

Chapter 3: Preparation and Physiochemical Characterization of Magnesium Phosphate Nanoparticles with Cationic Lipid coating for Intracellular Delivery of Cytochrome C (CytC LP/MgP)

3.1 Materials

Magnesium chloride (Acros Organics), trisodium phosphate (Mallinckrodt Chemical), cyclohexane (EMD Millipore), Triton-X100 (EMD Millipore), 1-hexanol (Alfa Aesar), sodium citrate (J. T. Baker Chemical), absolute ethanol (Fisher Scientific), sulfuric acid (Acros), hydrogen peroxide 35% (Sigma-Aldrich), silica gel (Alfa Aesar), ammonium molybdate tetrahydrate (Sigma-Aldrich), Ascorbic acid (Acros Organics), phosphorous standard (Ricca Chemical), cytochrome c (MP Biomedicals), 1,2-dioleoyl-3-trimethylammonium-propane (DOTAP) (Avanti Polar Lipids), cholesterol (Sigma-Aldrich), and HEPES (Fisher Scientific) were used as purchased without further purification.

3.2 Methods

3.2.1 Preparation and Characterization of Cytochrome C-encapsulated Cationic Liposomes (CytC LP)

Preparation of cytochrome c-encapsulated liposomes. Cytochrome c powder with different weight was dissolved in 1 ml pH 7.4, 5 mM HEPES buffer to obtain cytochrome c solution with different concentration. Aliquots of 156.48 µL 35.79 mM DOTAP and 74.24 µL 32.33 mM cholesterol solutions in chloroform, which were in the 7:3 molar ratio to yield a mixture of 8 µmol total lipids, were added into a Pyrex glass

tube, and then evaporated by a rotary evaporator at room temperature for 15 minutes to form a lipid film. The lipid film was placed under high vacuum for at least 4 hours to remove the residual solvent. The dried lipid film was hydrated with 0.7 mL cytochrome c solution and mildly vortexed for 20 seconds at room temperature to obtain a suspension of cytochrome c-encapsulated liposomes. The suspension was extruded 13 times through 100 nm polycarbonate membrane (Nucleopore, Pleasanton, CA) by a Mini-Extruder (Avanti Polar Lipids, Alabaster, AL) at room temperature to yield cytochrome c-encapsulated liposomes of smaller and more homogenous size.

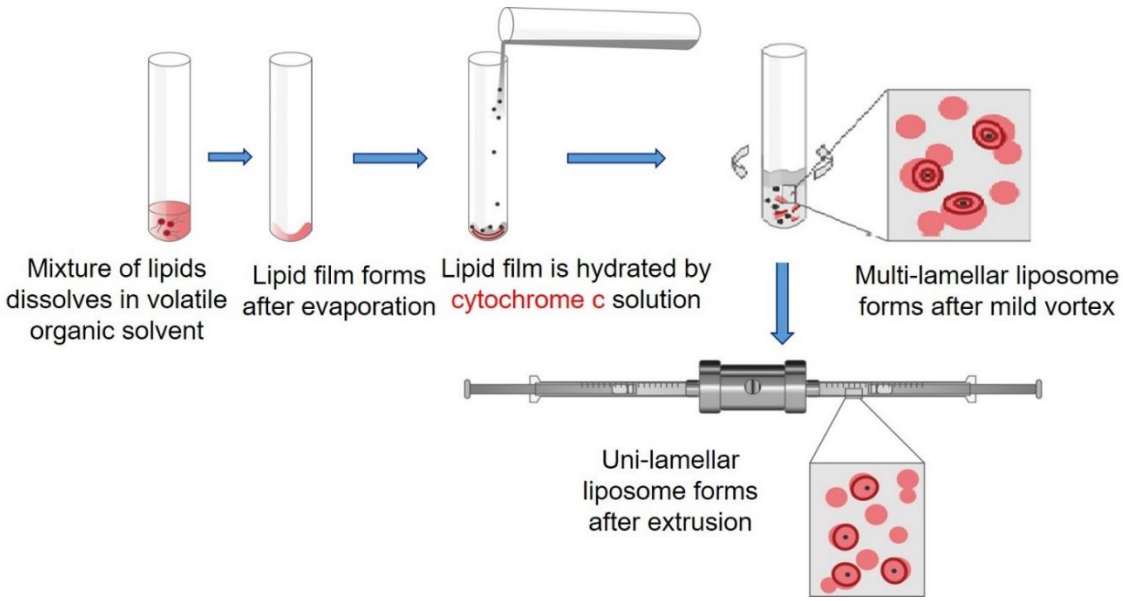

Fig. 3.1. Preparation of cytochrome c-encapsulated cationic liposomes.

Size and ζ-potential measurements of cytochrome c-encapsulated liposomes.

A 50-µL suspension of cytochrome c-encapsulated liposomes (CytC LP) was carefully added into a 10-mm square polystyrene cuvette (SARSTEDT, Germany) without creating

any air bubble. The cuvette was closed with a lid, slightly agitated and placed into a Malvern Zetasizer for size measurements. The temperature was maintained at 25 ℃.

After size measurements, the suspension in the cuvette was diluted into 1 mL pH 7.4, 5 mM HEPES buffer and the ζ-potential was measured immediately. The diluted suspension was slowly infused into a folded capillary cell (Malvern Instruments, UK) without creating any air bubble. The volume of the diluted suspension was adequate to completely cover the electrodes of the cell. The two openings of the cell were closed with two lids and the cell was placed into the Malvern Zetasizer. The sample was equilibrated to 25 ℃ before measurements.

All the samples were measured in triplicates and the data were reported as mean ± standard deviation of the triplicate measurements.

TEM imaging. The TEM was performed at the Electron Imaging Facility, Department of Molecular and Cellular Biology, UC Davis with the help from Dr. Fei Guo. Briefly, a 5-µL the suspension of cytochrome c-encapsulated liposomes (CytC LP) was dropped onto a Pure Carbon Film Copper TEM grid on 400 mesh (TED PELLA INC., Redding, California). The suspension on the gird was air-dried for about 1 minute and the excess fluid was blotted away with filter paper. A few drops of uranyl acetate were then applied to the grid to generate a thin film of the suspension on the TEM grid, which was then immediately transferred onto a JEOL-1230 microscope for imaging at an accelerating voltage of 100 kV. The digital images were recorded and analyzed with EMMENU4 (TIETZ imaging software).

3.2.2 Preparation and Characterization of Magnesium Phosphate Nanoparticles (MgP)

Preparation of MgP nanoparticles. Magnesium phosphate nanoparticle (MgP) was prepared by micro-emulsion precipitation. A 15-mL mixture of organic solvents consisting of 75% cyclohexane, 15% Triton-X100 and 10% hexanol was added each into two round bottom flasks and stirred for 15 minutes. An aliquot (300 µl) of 333.33 mM $MgCl_2$ aqueous solution was added into one flask and another 300 µl 500 mM Na_3PO_4 aqueous solution into the other flask. The two mixtures were each stirred continuously for 30 minutes to form reverse water-in-oil (w/o) microemulsions. The Na_3PO_4 microemulsion was promptly added into the $MgCl_2$ microemulsion followed by another 30 minutes of continuous stirring to generate MgP nanoparticles. Sodium citrate (250 µL, 15 mM aqueous solution) was then added dropwise into the microemulsion to endow the MgP nanoparticles with negative surface charges. The mixture was then stirred for another 15 minutes until the microemulsion turned translucent.

For the separation of the MgP nanoparticles, 4 g silica gel (60-200 mesh) was suspended in 30 mL ethanol. The afore prepared microemulsion containing the MgP nanoparticle was poured into the silica gel-ethanol mixture with continuous stirring for 15 minutes to break the microemulsion and to adsorb the magnesium phosphate (MgP) nanoparticles onto the silica gel. Organic solvents were washed away with 200 mL ethanol and magnesium phosphate nanoparticles were then sequentially eluted with 15 mL 75% ethanol, 15 mL 50% ethanol, and two 15 mL 25% ethanol in water. The eluted nanoparticles were collected in eight 7.5 mL fractions. Suspensions of MgP nanoparticles in water were obtained after removing ethanol by rotary evaporation. The

entire process was carried out at 4ºC temperature, and the MgP nanoparticles were quantified using the phosphorous assay as detailed in the following section.

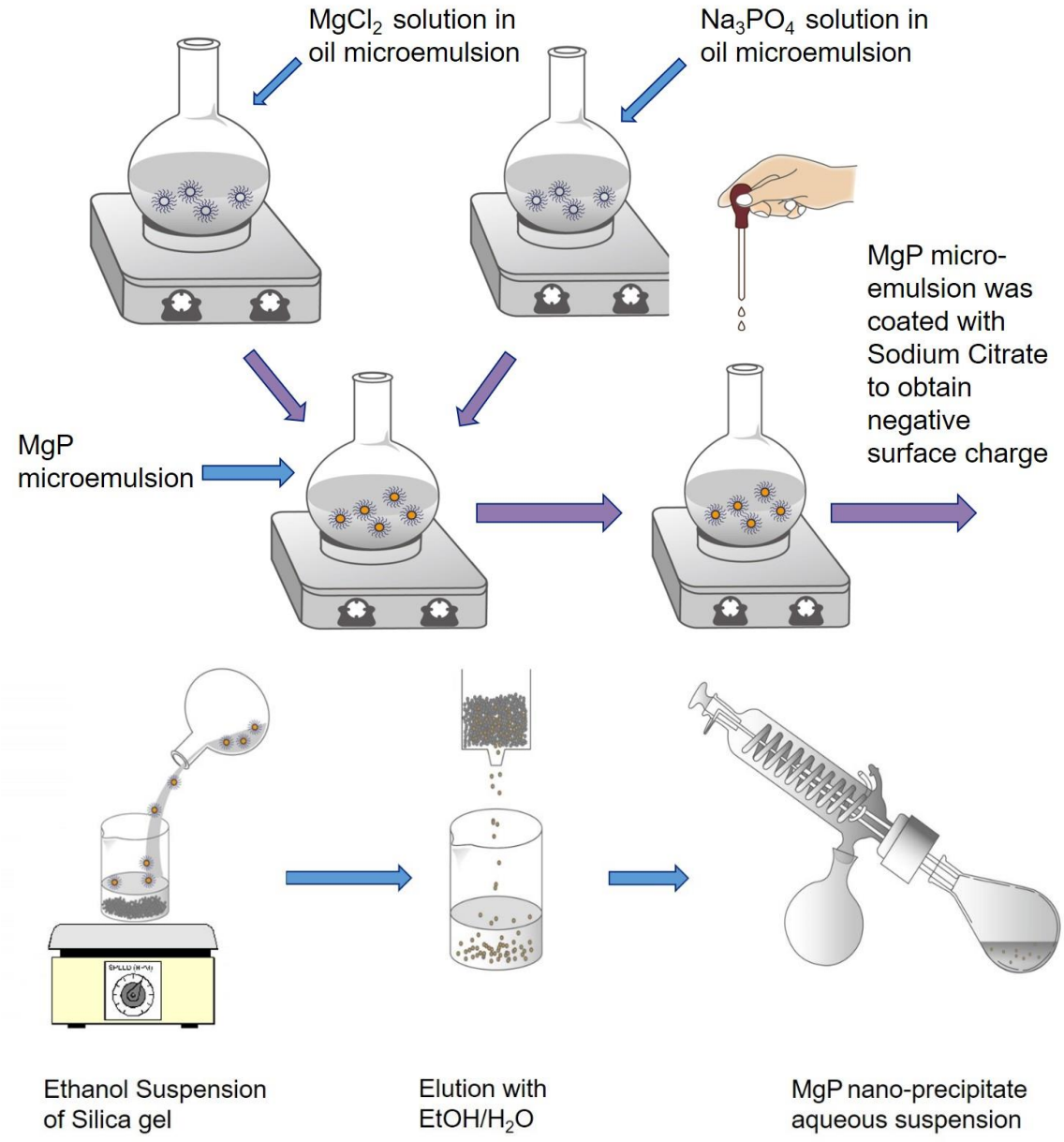

Fig. 3.2. Preparation of MgP nanoparticles.

Phosphorus assay. 10 N H_2SO_4 was prepared by carefully adding 1 mL stock 35 N H_2SO_4 to 2.5 mL deionized water. 10% H_2O_2 was prepared by mixing 1 mL stock 35% H_2O_2 with 2.5 mL deionized water. Molybdate reagent was prepared by dissolving 0.22 g ammonium molybdate tetrahydrate in 2.5 mL of 10 N H_2SO_4, followed by dilution with deionized water to 100 mL. 10% ascorbic acid solution was obtained by dissolving 5 g ascorbic acid in 50 g deionized water.

For the preparation of standards, 6 different volumes of a phosphorus standard solution were placed into 6 different clean Pyrex tubes as follows: 0 nmol (0 µL) as blank, 125 nmol (77.5 µL), 250 nmol (155 µL), 375 nmol (232.5 µL), 500 nmol (310 µL), and 625 nmol (387.5 µL).

For each sample, 20 µL of a suspension of MgP nanoparticle was placed into the bottom of a Pyrex tube. An aliquot (0.4 mL) of 10 N H_2SO_4 was added to each sample and standard. All tubes were then heated in a solid anodized aluminum block in the fume hood at 200-210 ℃ for 60 minutes. The tubes were removed from the block and allowed to cool for 10 minutes at room temperature. An aliquot (0.1 mL) of 10% H_2O_2 was added to each tube. All tubes were heated again at 190-210 ℃ for 10 minutes and then cooled at room temperature for 10 minutes. The molybdate reagent (4.7 mL) and 10% ascorbic acid (0.5 ml) were added to each tube and all tubes were vortexed immediately for 10 seconds. All tubes were then heated at 100 ℃ for 10 minutes, when blue color was observed in tubes containing substantial phosphate. The tubes were then cooled on the ice to reach room temperature rapidly. The UV absorbance at 800 nm was then determined by UV-visible spectrophotometer, UV-1601 (Shimadzu, Japan) after the standard tube containing 0 nmol phosphate used to manually adjust the absorbance to zero. A

calibration curve was generated using the absorbance of standard samples and used to determine the amount of phosphorus in unknown samples.

Size and ζ-potential measurements of MgP nanoparticles. An aliquot (50 μL) of a suspension of MgP nanoparticles was carefully added into a 10-mm square polystyrene cuvette (SARSTEDT, Germany) without creating any air bubble. The cuvette was closed with a lid, slightly agitated and placed into the Malvern Zetasizer. The temperature was maintained at 25 ℃.

After size measurements, the suspension in the cuvette was diluted to 1 mL using deionized water and the ζ-potential was measured immediately. The diluted suspension was slowly infused into a folded capillary cell (Malvern Instruments, UK) without creating any air bubble. The volume of the diluted suspension was adequate to completely cover the electrodes of the cell. The two openings of the cell were closed with two lids and was placed into the Zetasizer. The sample was equilibrated to 25 ℃ before measurements.

All the measurements were in triplicate and the data were reported as mean ± standard deviation of the triplicates.

TEM imaging. The TEM was performed at the Electron Imaging Facility, Department of Molecular and Cellular Biology, UC Davis with the help from Dr. Fei Guo. Briefly, a 5-μL the suspension of magnesium phosphate nanoparticles (MgP) was dropped onto a Pure Carbon Film Copper TEM grid on 400 mesh (TED PELLA INC., Redding, California). The suspension on the gird was air-dried for about 1 minute and the excess fluid was blotted away with filter paper. The thin film of the suspension on the TEM grid was then immediately transferred onto a JEOL-1230 microscope for

imaging at an accelerating voltage of 100 kV. The digital images were recorded and analyzed with EMMENU4 (TIETZ imaging software).

3.2.3 Wrapping of Magnesium Phosphate Nanoparticles with Cytochrome C-encapsulated Cationic Liposomes (CytC LP/MgP)

Preparation of MgP nanoparticles coated with cytochrome c-encapsulated liposomes. The phosphoric concentration of MgP nanoparticles was determined by the previous phosphorus assay so that the amount of MgP nanoparticles to be mixed with CytC LP matched a 7:3 molar ratio between the amount of total lipids in CytC LP and the amount of phosphorus in MgP nanoparticles. The amount of MgP nanoparticles to be added to the CytC LP was determined based on the phosphorus assay, and the corresponding volume of the suspension of MgP nannoparticles was mixed with CytC LP for 1 hour at room temperature. Appropriate volume of pH 7.4, 5 mM HEPES buffer was used to dilute CytC solution to reach an appropriate concentration.

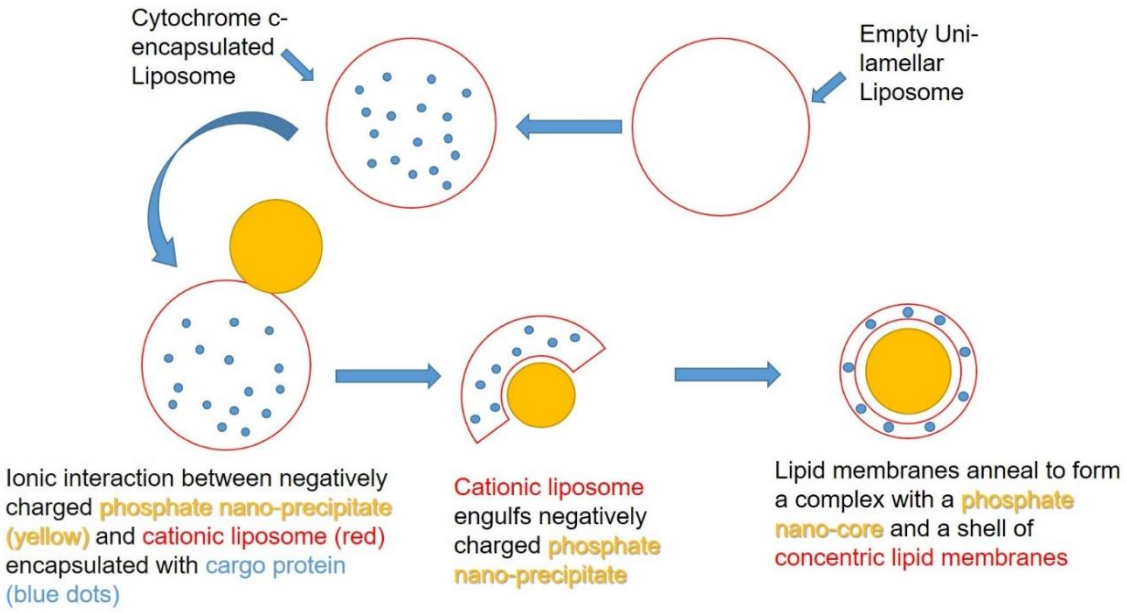

Fig. 3.3. Spontaneous wrapping of negatively charged MgP nanoparticles by cationic liposomes.

Size and ζ-potential measurements of cytochrome c-encapsulated liposomes with MgP nanoparticles. An aliquot (50 μL) of a suspension of cytochrome c-encapsulated liposomes with MgP nanoparticles (CytC LP/MgP) was carefully added into a 10-mm square polystyrene cuvette (SARSTEDT, Germany) without creating any air bubble. The cuvette was closed with a lid, slightly agitated and placed into the Malvern Zetasizer. The temperature was maintained at 25 ℃.

After size measurements, the suspension in the cuvette was diluted to 1 mL using deionized water and the ζ-potential was measured immediately. The diluted suspension was slowly infused into a folded capillary cell (Malvern Instruments, UK) without creating any air bubble. The volume of the diluted suspension was adequate to completely cover the electrodes of the cell. The two openings of the cell were closed

with two lids and was placed into the Zetasizer. The sample was equilibrated to 25 ℃ before measurements.

All the measurements were in triplicate and the data were reported as mean ± standard deviation of the triplicates.

TEM imaging. The TEM was performed at the Electron Imaging Facility, Department of Molecular and Cellular Biology, UC Davis with the help from Dr. Fei Guo. Briefly, a 5-µL the suspension of cytochrome c-encapsulated liposomes with MgP nanoparticles (CytC LP/MgP) was dropped onto a Pure Carbon Film Copper TEM grid on 400 mesh (TED PELLA INC., Redding, California). The suspension on the gird was air-dried for about 1 minute and the excess fluid was blotted away with filter paper. A few drops of uranyl acetate were then applied to the grid to generate a thin film of the suspension on the TEM grid, which was then immediately transferred onto a JEOL-1230 microscope for imaging at an accelerating voltage of 100 kV. The digital images were recorded and analyzed with EMMENU4 (TIETZ imaging software).

3.3 Results

3.3.1 Phosphorus Assay

The phosphate in the proposed formulation is important for buffering the protons, and thus for preventing the acid-induced protein denaturation. The phosphate also contributes to the high osmotic pressure from the dissolved MgP. The MgP nanoparticles are quantified using the phosphorus assay. The concentration of phosphate ions in a fraction of nanoparticle is quantified based on a colorimetric method.

In the gradient elution of MgP nanoparticles, the concentration of phosphates in the eluant fractions depended on the percentage of water in the eluting solvent. The

result (Fig. 3.4.) shows that the concentration of phosphates in the second fraction that was eluted with 25% ethanol in water was the highest at 24.53±3.22 nmol/mL. It is advisable to perform this assay every time in order to quantify phosphates present in the sample.

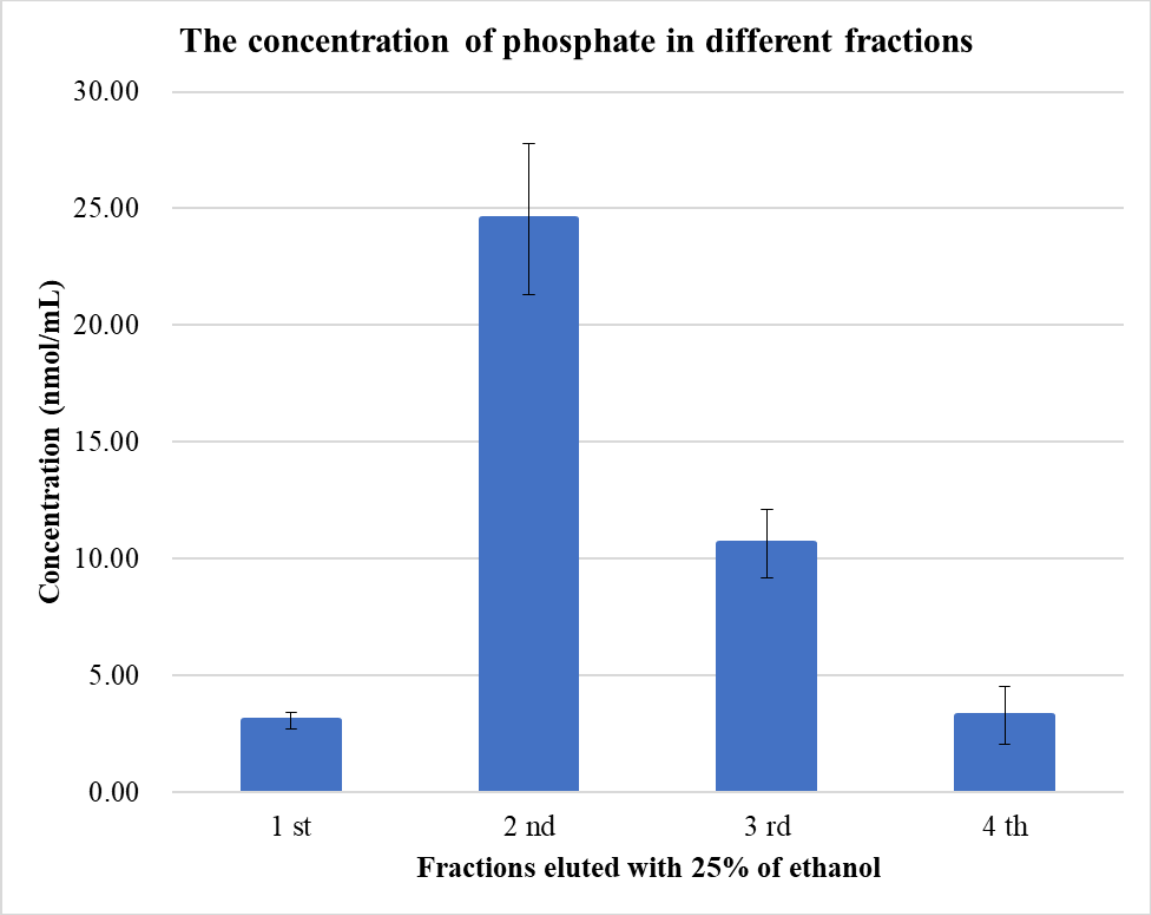

Fig. 3.4. Concentration of phosphate in fractions eluted with 25% of ethanol collected from chromatograph.

The eluted MgP nanoparticles were collected in eight 7.5 mL fractions. Two fractions each were collected after elution with 75% and 50% ethanol. Four fractions

were collected after elution with 25% ethanol. Majority of phosphate concentrated in the second fraction of the eluent generated with 25% ethanol.

The initial preparation of MgP nanoparticles used 500 mM $MgCl_2$ and 500 mM $(NH_4)_2HPO_4$ aqueous solutions. The resultant mixed precipitates of dibasic magnesium phosphate trihydrate (newberyite, $MgHPO_4 \cdot 3(H_2O)$) and cattiite ($Mg_3(PO_4)_2 \cdot 22H_2O$) at pH 7.4, 4 ℃ [24], and a Mg^{2+}:PO_4^{3-} ratio of 1:1 showed relatively low phosphorous concentration of 7.79±0.93 nmol/mL in the second fraction that was eluted with 25% ethanol (Fig. 3.5.).

Alternatively, 333.33 mM $MgCl_2$ and 500 mM Na_2HPO_4 aqueous solutions were mixed in a physiological molar ratio of Mg^{2+}:PO_4^{3-} = 2:3. Although the same mixed precipitates were produced [24], the resultant MgP nanoparticles showed a relatively high phosphate concentration of 19.88±2.93 nmol/mL in the second fraction that was eluted with 25% ethanol (Fig. 3.5.).

As another alternative, 333.33 mM $MgCl_2$ and 500 mM Na_3PO_4 aqueous solutions were mixed in a physiological molar ratio of Mg^{2+}:PO_4^{3-} of 2:3, which only formed cattiite ($Mg_3(PO4)_2 \cdot 22H_2O$) precipitates at pH 7.4, 4 ℃ [24]. Surprisingly, the resultant MgP nanoparticles showed a phosphate concentration of 24.53±3.22 nmol/mL in the second fraction that was eluted with 25% ethanol (Fig. 3.5.), which is a much higher phosphate concentration than the previous two conditions of making MgP nanoparticles.

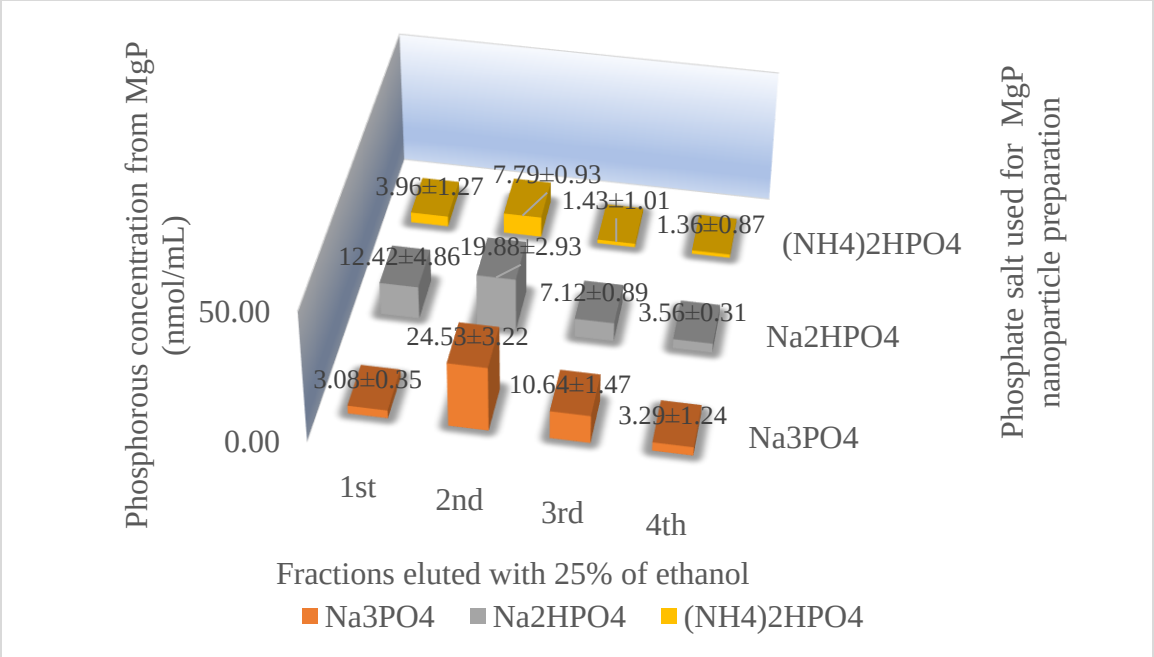

Fig. 3.5. Na_3PO_4 improved the phosphorous concentration in magnesium phosphate nanoparticles (MgP).

3.3.2 Colloidal Properties of MgP, CytC LP and CytC LP/MgP

The result of size and surface charge measured by dynamic light scattering (DLS) (Table 3.1.) shows that the average diameter of both CytC LP and CytC LP/MgP were around 150 nm. Surprisingly, the size distribution by volume of MgP showed two peaks, which will be discussed later. The ζ-potential changed with compositions of the colloid, from -9.58 mV of negatively charged MgP, to 48.1 mV of CytC LP due to the cationic lipids, and then to 27.2 mV of the final formulation of CytC LP/MgP that was made of both MgP and CytC LP.

Table 3.1. Size and ζ -potential of MgP, CytC LP and CytC LP/MgP.

	Size (nm)	**PDI**	**ζ-Potential (mV)**
CytC LP	124.6±38.70	0.058	48.1±9.80
MgP	61.08±9.915 380.7±96.47 (two peaks)	0.362	-9.58±4.13
CytC LP/MgP	158.0±64.17	0.099	27.2±7.30

Each value represents the mean±S.D. of at least three experiments.

3.3.3 TEM Imaging of MgP, CytC LP and CytC LP/MgP

Fig. 3.6. (A) shows that most MgP nanoparticles in TEM images matched the first peak in the size distribution of MgP as measured by DLS. This phenomenon will be discussed later. The other finding is that although the electrostatic repulsion brought by sodium citrate kept nanoparticles separated, some MgP still stuck together.

Fig. 3.6. (B) shows that the cargo protein cytochrome c was encapsulated into CytC LP.

Fig. 3.6. (C) is the TEM image of CytC LP/MgP. MgP nanoparticles were in the center of liposomes as expected.

A

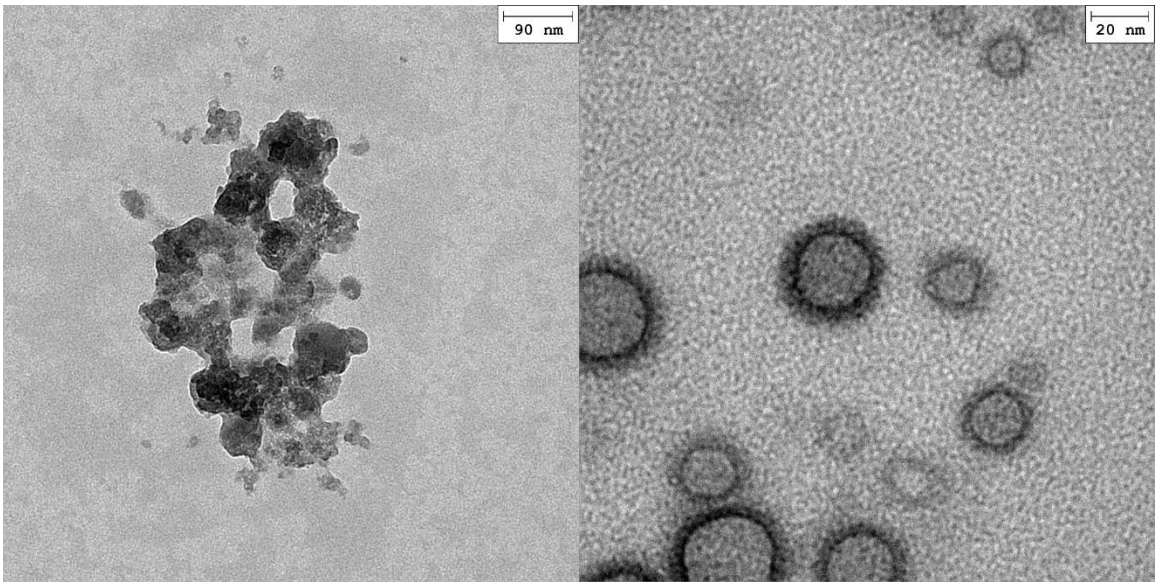

B

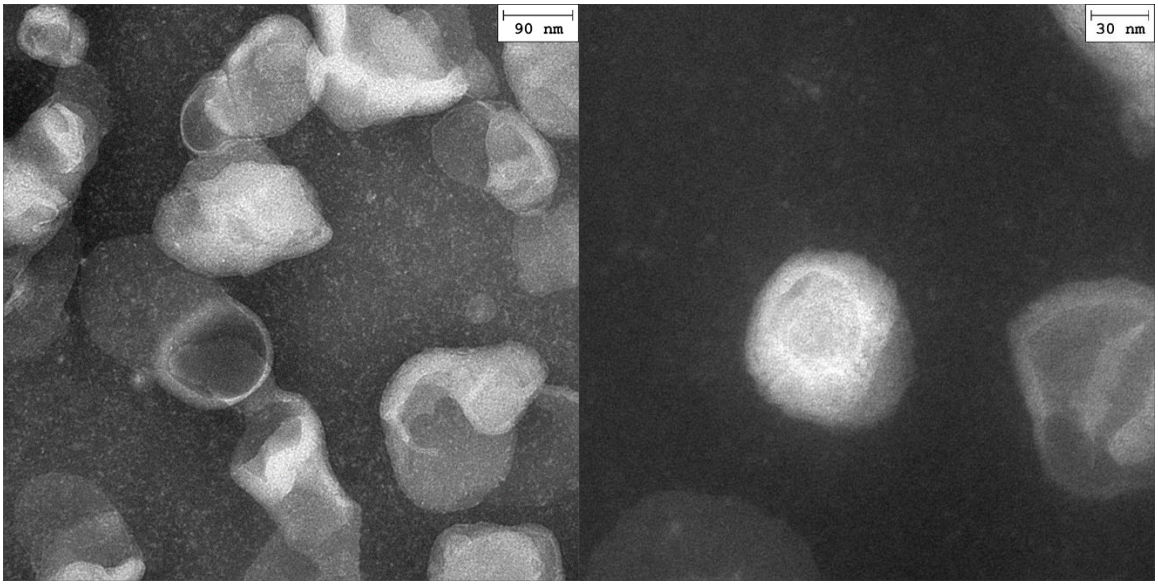

C

(with negative staining) **(without negative staining)**

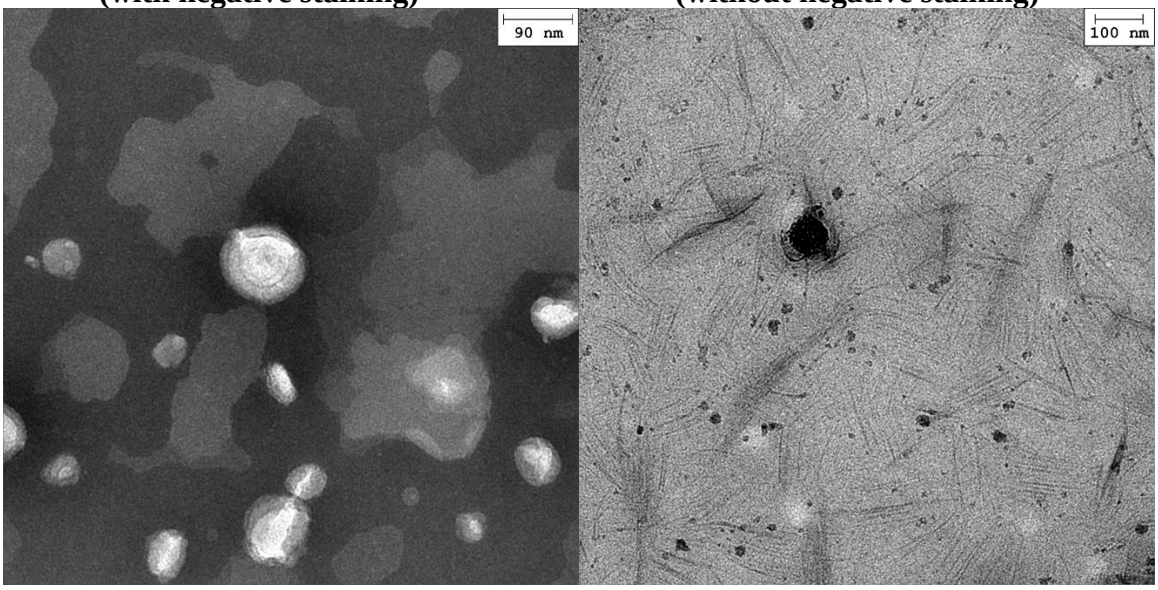

Fig. 3.6. TEM images of (A) MgP, (B) CytC LP, and (C) CytC LP/MgP.

3.4 Discussion

3.4.1 MgP Produced by the Strategy of Microfluidic Mixing

The NanoAssemblr Benchtop (Precision Nanosystems, Vancouver, BC) is a nanoparticle synthesis system, whose proprietary microfluidics technology enables controlled, bottom-up, molecular self-assembly of nanoparticles through millisecond mixing of components at nanoliter scale. This technique is time-saving and allows large-scale preparation of MgP nanoparticles within one day. However, the best result (Fig. 3.6.) of MgP preparation with a size of 79.61±25.82 nm in diameter and a ζ-potential of -8.00±7.28 mV was not reproducible. Consequently, the micro-emulsion method was eventually elected over this alternative method.

Results

		Size (d.nm):	% Intensity:	St Dev (d.n...
Z-Average (d.nm): 72.70	Peak 1:	79.61	100.0	25.82
PdI: 0.122	Peak 2:	0.000	0.0	0.000
Intercept: 0.925	Peak 3:	0.000	0.0	0.000

Result quality : Good

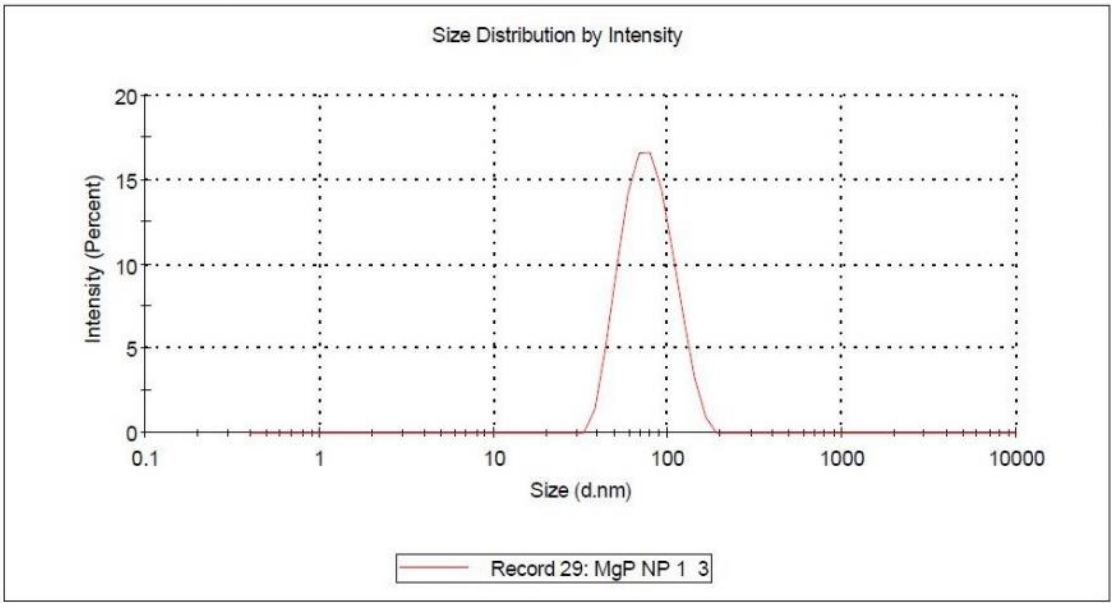

Fig. 3.7. The most optimized size of MgP generated by the NanoAssemblr Benchtop.

3.4.2 Comparison of DLS and TEM Characterizations of CytC LP/MgP

Dynamic light scattering (DLS) measures the size and surface zeta potential of small particles. Brownian motion of water molecules moves small, suspended particles in and out of the detection of their scattered light to cause fluctuation of the scattered light intensity. The fluctuation can then be used to calculate the hydrodynamic diameter of the particles. DLS is convenient and can detect a large population of the particles in the suspension. However, DLS cannot measure the size of the particle core, the size of varied surface structures, and is limited by the particle concentration.

Transmission electron microscope (TEM) can be used to examine details of the structure of a formulation, such as aggregations and cores with a simple sample preparation. TEM is not easily accessible in common labs and quantitation of the size of particles need to sample an enormous number of images, which is time-consuming and inconvenient.

As shown in Fig. 3.8., two peaks were observed in the DLS analysis of the size of MgP nanoparticles. The first peak showed the hydrodynamic diameter of 61.08±9.915 nm, which possessed 56.2% by volume, indicating this is the diameter that reflect the size of most of the MgP nanoparticles. The second peak showed the size of 380.7±96.47 nm, which possessed 43.8% by volume, suggesting that MgP might undergo aggregation.

Results

			Size (d.nm):	% Volume:	St Dev (d.nm):
Z-Average (d.nm):	330.3	**Peak 1:**	380.7	43.8	96.47
PdI:	0.362	**Peak 2:**	61.08	56.2	9.915
Intercept:	0.910	**Peak 3:**	0.000	0.0	0.000

Result quality : Refer to quality report

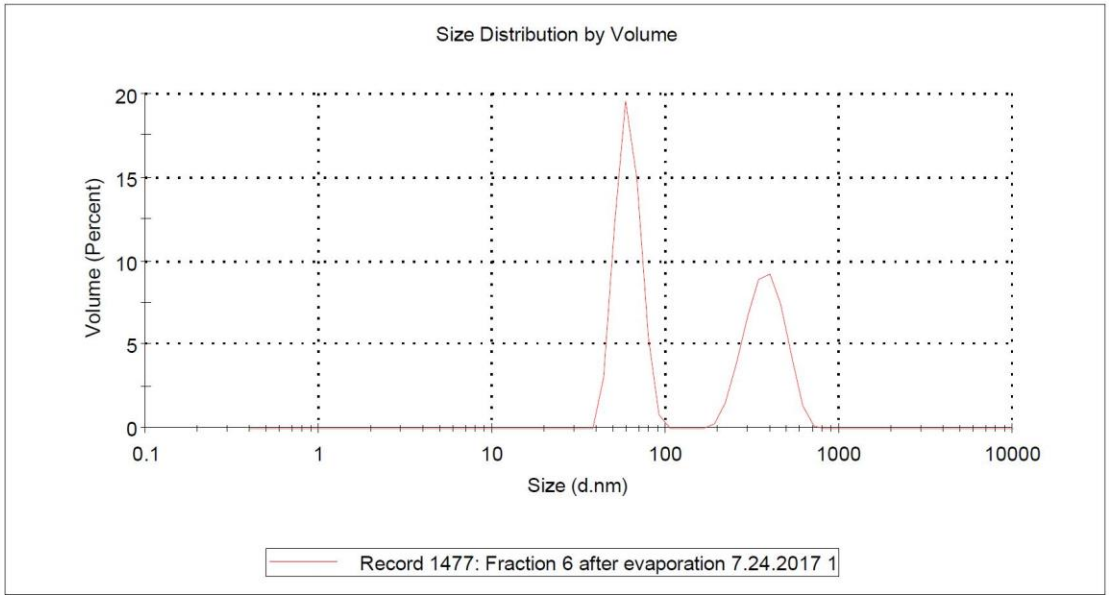

Fig. 3.8. Size distribution by volume of MgP measured by DLS.

As shown in Fig. 3.6. (A), the aggregation of MgP nanoparticles were directly observed by TEM. Despite the addition of sodium citrate, the ζ-potential of MgP was only slightly negative around -10 mV whereas a surface charge of either higher than +30 mV or lower than -30 mV is needed keep the particles stable in a suspension. Because of this, the particles of MgP could not sufficiently repulse one another by electrostatic force to prevent aggregation.

DLS studies showed two peaks of 380.7±96.47 nm and 61.08±9.915 nm in hydrodynamic diameter for MgP, one peak of 124.6±38.70 nm for CytC LP, and one peak of 158.0±64.17 nm for the final formulation of CytC LP/MgP. From TEM image (Fig. 3.6. (C)), the size of the final formulation of CytC LP/MgP was around 100 nm,

which was still in the range of size distribution by volume of DLS. There were two possible reasons to explain why the size of final CytC LP/MgP (Fig. 3.9.) was not close to the predominant size of MgP around 61.08 nm: 1) from Fig. 3.6. (C), liposomes engulfed more than one MgP nanoparticles in the core to give to a larger size of final CytC LP/MgP; 2) lipid membranes loosely wrapped around the MgP nano-core, to form a relatively thick liposomal shell. Further TEM investigation is needed to confirm these speculations.

From TEM image (Fig. 3.6. (C)), CytC LP/MgP carrying a magnesium phosphate nano-core, a coating of lipid membranes encapsulated with cargo protein CytC was successfully prepared. There was a mechanism how the interaction happened between inorganic nanoparticles and lipid membranes: engulfment of negatively charged MgP with cationic CytC LP, which can be reflected on the change of ζ-potential. When the engulfment happened, the ζ-potential changed from 48.1 mV on CytC LP to 27.2 mV on the final formulation of CytC LP/MgP, which can be explained by the disproportional distribution of positive charges to the inside of CytC LP/MgP due to the electrostatic interaction between a large amount of positive charges on lipid membranes and negatively charged MgP, leading to the decrement of the density of positive charges outside of CytC LP/MgP.

Results

		Size (d.nm):	% Volume:	St Dev (d.nm):
Z-Average (d.nm): 164.5	Peak 1:	158.0	100.0	64.17
PdI: 0.099	Peak 2:	0.000	0.0	0.000
Intercept: 0.902	Peak 3:	0.000	0.0	0.000

Result quality : Good

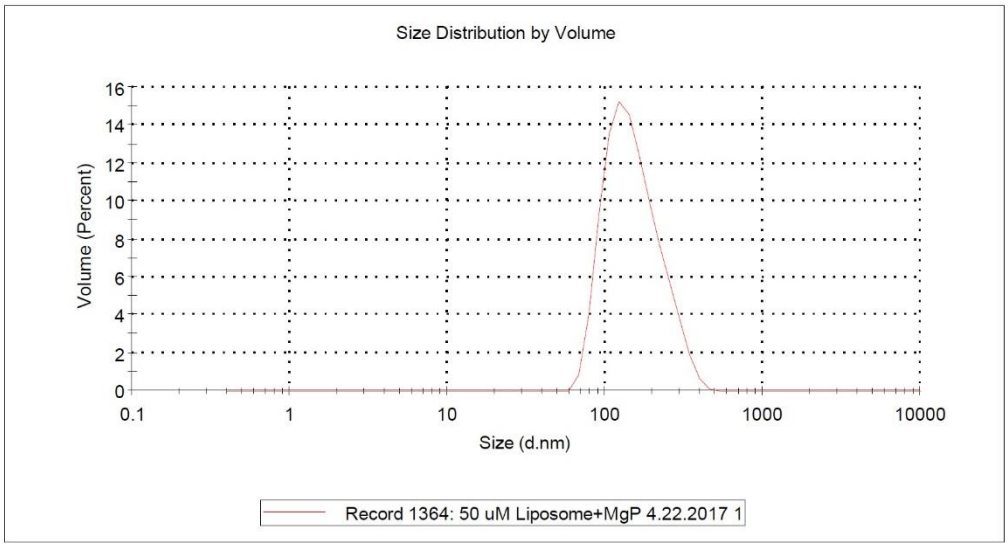

Fig. 3.9. Volume distribution of the size of CytC LP/MgP per DLS.

3.5 Conclusion

CytC LP/MgP was successfully prepared and its physicochemical properties were characterized. CytC LP/MgP had the approximate size of 150 nm in diameter and the surface charge around 30 mV.

Chapter 4: Characterization of Cationic Liposome-coated Magnesium Phosphate Nanoparticles for Intracellular Delivery of Cytochrome C (CytC LP/MgP) into Lung Cancer Cells A549

4.1 Introduction

A549, a lung adenocarcinoma cell line belongs to non-small cell lung cancer (NSCLC), which accounts for 40% of all lung cancers. Adenocarcinoma occurs mainly in current and former smokers, but is also the most common type of lung cancer seen in non-smokers. Adenocarcinoma is more common in women than in men and is more likely to occur in young people than other types of lung cancer [25]. Cytochrome c (CytC) is a potential anticancer protein that may induce apoptosis by the mitochondrial pathway. Cellular uptake of CytC in different formulations was monitored by green-fluorescent dye Alexa Fluor® 488 that can be conjugated to the protein. The MTS Assay on cell viability was conducted to study the cell killing effect of CytC LP/MgP in A549 cells.

4.2 Materials

A549 cells were purchased from ATCC, cytochrome c (MP Biomedicals), DMEM/F-12, 50/50, 1X (Corning), fetal bovine serum (Gemini), penicillin-streptomycin solution (Cellgro), L-glutamine(Cellgro), trypsin 0.25% (1X) (HyClone), Alexa Fluor™ 488 carboxylic acid, succinimidyl ester (Thermo Fisher Scientific), DMSO (Fisher

Scientific), PBS with 1 M NaCl solution (Santa Cruz Biotechnology), MitoRed (PromoKine), PBS, 1X (Corning), 4% paraformaldehyde in phosphate-buffered saline (Boston BioProducts), Hoechst 33342 (Thermo Scientific), RPMI medium 1640 (1X) (Gibco), CellTiter96® AQueous One solution cell proliferation assay (Promega) were purchased and used without further purification.

4.3 Methods

4.3.1 Fluorescence Imaging Analysis

The preparations of formulations. ***Conjugation of Alexa Fluor® 488 to cytochrome c (Alexa 488-labeled CytC).*** 10 mg of cytochrome c was dissolved in 1 mL of pH 8.3, 5 mM HEPES buffer. Alexa Fluor™ 488 NHS Ester (Succinimidyl Ester) was dissolved in DMSO at 10 mg/mL. While stirring or vortexing the cytochrome c solution, 75 µL of the reactive dye solution was slowly added. The reaction mixture was incubated for 1 hour at room temperature with continuous stirring. The conjugate was separated from unreacted labeling reagent using Amicon® Ultra 15 mL centrifugal filter (EMD Millipore, Billerica, MA) with 3 kDa molecular weight cutoff according to the following. The mixture of cytochrome c and dye was diluted to 4 mL with pH 7.4, 5 mM HEPES buffer. The diluted mixture was centrifuged at 4000 x g at 25 °C for 1 hour. The concentrate in the filter device sample reservoir was diluted to 4 mL again and then centrifuged for another 1 hour. The concentrate was diluted back to 2 mL to yield 245.14 µM Alexa Fluor® 488-labeled cytochrome c (Alexa 488-labeled CytC) solution. HEPES buffer (0.2 mL, 5 mM at pH 7.4) was added to dilute the resultant suspension of Alexa 488-labeled CytC to 146.95 µM.

Preparation of LP/MgP containing Alexa Fluor® 488-labeled cytochrome c (Alexa 488-labeled CytC LP/MgP). DOTAP (156.48 µL 35.79 mM) and cholesterol (74.24 µL 32.33 mM) solutions in chloroform were added into a Pyrex glass tube to yield a mixture of 8 µmol total lipids in 7:3 molar ratio. The organic solvent of the mixture was evaporated by a rotary evaporator at room temperature for 15 minutes to form a lipid film, which was placed under high vacuum condition for at least 4 hours to remove the residual solvent. The dried lipid film was hydrated with 0.7 mL of 245.14 µM Alexa Fluor® 488-labeled cytochrome c solution and mildly vortexed for 20 seconds at room temperature to obtain a suspension of liposomes containing Alexa Fluor® 488-labeled cytochrome c (Alexa 488-labeled CytC LP). The suspension was extruded 13 time through 100 nm polycarbonate membrane (Nucleopore, Pleasanton, CA) by a Mini-Extruder (Avanti Polar Lipids, Alabaster, AL) at room temperature. Based on the phosphorus assay, 138.46 µL of MgP nanoparticles, which carried the phosphoric concentration of 10.61 mM, was mixed with 0.3 mL of Alexa 488-labeled CytC LP, followed by incubation for 1 hour at room temperature. Size and ζ-potential of Alexa 488-labeled CytC LP with MgP nanoparticles (Alexa 488-labeled CytC LP/MgP) were measured by the Zetasizer, when 61.54 µL of pH 7.4, 5 mM HEPES buffer was added to obtain 146.95 µM Alexa Fluor® 488-labeled CytC, 6.85 mM total lipids, and 2.94 mM phosphate from MgP in the final formulation.

Preparation of Alexa Fluor® 488-labeled cytochrome c-complexed with MgP nanoparticles (Alexa 488-labeled CytC+MgP). Based on the phosphorus assay, 138.46 µL of MgP nanoparticles, which carry the phosphoric concentration was 10.61 mM, was mixed with 0.3 mL of Alexa 488-labeled CytC, followed by incubation for 1 hour at

room temperature. Size and ζ-potential of Alexa Fluor® 488-labeled cytochrome c-complexed with MgP nanoparticles (Alexa 488-labeled CytC+MgP) were measured by the Zetasizer, for which 61.54 µL of pH 7.4, 5 mM HEPES buffer was added to obtain 146.95 µM Alexa Fluor® 488-labeled CytC and 2.94 mM phosphate from MgP in the final formulation.

Preparation of bare cationic liposomes (bare LP). DOTAP (156.48 µL 35.79 mM) and cholesterol (74.24 µL 32.33 mM) solutions in chloroform were added into a Pyrex glass tube to yield a mixture of 8 µmol total lipids in 7:3 molar ratio. The organic solvent of the mixture was evaporated by a rotary evaporator at room temperature for 15 minutes to form a lipid film, which was placed under high vacuum condition for at least 4 hours to remove the residual solvent. The dried lipid film was hydrated with 0.7 mL of pH 7.4, 5 mM HEPES buffer solution and mildly vortexed for 20 seconds at room temperature to obtain a suspension of bare cationic liposomes (bare LP). The suspension was extruded 13 time through 100 nm polycarbonate membrane (Nucleopore, Pleasanton, CA) by a Mini-Extruder (Avanti Polar Lipids, Alabaster, AL) at room temperature. Size and ζ-potential of bare LP were measured by the Zetasizer. HEPES buffer (0.2 mL, 5 mM at pH 7.4) was added to dilute the resultant suspension of bare LP to 6.85 mM.

Preparation of bare cationic liposomes with MgP nanoparticles (bare LP/MgP). Based on the phosphorus assay, 138.46 µL of MgP nanoparticles, which carry the phosphoric concentration of 10.61 mM, was mixed with 0.3 mL of cationic, followed by incubation for 1 hour at room temperature. Size and ζ-potential of bare cationic liposomes with MgP nanoparticles (bare LP/MgP) were measured by the Zetasizer, for

which 61.54 µL of pH 7.4, 5 mM HEPES buffer was added to obtain the final formulation.

The preparation of stock solution of MitoRed for mitochondrial staining. To prepare a 200 µM stock solution, 50 µg vial of MitoRed powder was dissolved in 460 µL anhydrous DMSO.

The preparation of Hoechst 33342 working solution for nuclear staining. A dilution of Hoechst 33342 was prepared in PBS for a final concentration of 1 mg/mL. The resultant solution was diluted to 1 µg/mL in PBS for nuclear staining.

The preparation of cell culture and staining. The A549 cells were grown in Dulbecco's Modified Eagle Medium: Nutrient Mixture F-12, 1:1 (DMEM/F-12, 1:1) medium, supplemented with 10% fetal bovine serum (FBS), 1% antibiotics (penicillin 5000 U/mL, and streptomycin 5000 µg/mL) and 1% L-glutamine. A549 cells were seeded in two 6-well plates (Ultra Cruz™, Santa Cruz Biotechnology) at a density of 2 x 10^5 cells/well and incubated under the condition of 5% CO_2 at 37 ℃ overnight (12 hours) to obtain 50% - 80% confluence.

The wells with or without cells were treated with 2 mL of different formulations pre-diluted with culture medium to obtain 14.69 µM Alexa Fluor® 488-labeled CytC, 0.685 mM lipids, or 0.294 mM MgP in formulations. After incubation at 37 ℃ for three hours, cells were washed once with PBS with 1 M NaCl solution for several seconds.

For the staining of mitochondria, MitoRed was diluted to 200 nM in pre-warmed culture medium. PBS in cell wells was removed and 1 mL of the diluted MitoRed solution was added into each well. Cells were incubated for 30 minutes at 37 ℃. The

MitoRed solution was removed and cells were washed with culture medium once and PBS once, each time for 3 minutes with the benchtop orbital shaker.

For fixation, cells were first washed with PBS. PBS was then removed followed by addition of pre-warmed 4% paraformaldehyde (PFA) solution in PBS. Cells were incubated for 17 minutes, and then washed with PBS twice for 3 minutes each time with a benchtop orbital shaker.

For the staining of nuclei, cells were washed with PBS. After removing PBS, 1 mL of 1 μg/mL Hoechst 33342 solution was added to completely cover the cells in each well. Aluminum foil was placed over the sample to protect it from light. Cells were incubated at room temperature for 5 minutes and washed twice with PBS for 3 minutes each time with the benchtop orbital shaker.

Fluorescence imaging assay. Fluorescent images were acquired with a fluorescence microscope BZ-X710 (KEYENCE, Japan). Exact same parameters (excitation light: 40%; objective lens: 4x; exposure time for BZ-X filter DAPI: 1/1.2 seconds; exposure time for BZ-X filter GFP: 3 seconds; exposure time for BZ-X filter TxRed: 3s) were set for imaging all 6 different treatments (Alexa 488-labeled CytC, Alexa 488-labeled CytC/MgP, bare LP/MgP, bare LP, Alexa 488-labeled CytC+MgP, and no treatment) and their control groups with no cells.

Images under different filters were taken from each well and digitally superimposed. The green fluorescence of the image _CH1 was from Alexa 488 labeled-CytC in A549 cells, the red fluorescence of the image _CH2 was from mitochondria in A549 cells, and the blue fluorescence of the image _CH3 was from nuclei in A549 cells.

Each fluorescence intensity was measured using ImageJ from National Institutes of Health (NIH) under the same thresholds.

4.3.2 Cell Viability Assay

A549 cells were grown in RPMI-1640 medium supplemented with 10% fetal bovine serum (FBS), 1% antibiotics (penicillin 5000 U/mL, and streptomycin 5000 μg/mL) and 1% L-glutamine.

A549 cells were seeded in 96-well plates (Ultra Cruz™, Santa Cruz Biotechnology) at a density of 5000 cells/well and incubated under 5% CO_2 at 37 ℃ overnight (12 hours) to obtain around 50% to 80% confluence. Cells were treated with 100 μL of 6 different formulations (Free CytC, CytC LP/MgP, bare LP, bare LP/MgP, MgP, and CytC+MgP). The formulations are prepared in the same way as those for the aforementioned fluorescence imaging assay, each applied at 8 different concentrations by pre-dilution with complete culture medium to carry 50, 10, 5, 1, 0.5, 0.1, 0.05 and 0.01 μM CytC, 428.47, 85.69, 17.14, 8.57, 4.28, 0.86, 0.43 and 0.09 μM total lipids, or 180, 36.7, 18.4, 3.67, 1.84, 0.367, 0.184, 0.0367 μM phosphate from MgP. After 48-hour incubation at 37 ℃, cells were washed twice with PBS, each time for 3 minutes with the benchtop orbital shaker.

Cell viability was measured by the MTS assay. 20 μL of CellTiter 96® AQueous One Solution Reagent was added into each well of the 96-well plate containing 100 μL culture medium without phenol red. After 4 hours of incubation at 37 ℃, the absorbance of all the contents at 490 nm was measured by Biotek Synergy HT Multimode microplate reader (BioTek Instruments, Winooski, VT). The absorbance of cells without any

treatment was taken as 100% viability, and the absorbance of wells containing medium but without cells was taken as background.

Cell viability was calculated by the following formula:

$\text{Cell Viability } [\%] = \frac{\text{OD}_{490}\text{ sample} - \text{OD}_{490}\text{ background}}{\text{OD}_{490}\text{ control} - \text{OD}_{490}\text{ background}} \times 100\%$, where OD_{490} sample is the UV absorbance of cells treated with a formulation at an aforementioned concentration, OD_{490} control is the UV absorbance of cells treated with no formulation but growth media as a control for 100% viability, and OD_{490} background is the UV absorbance of wells with media but no cells.

Dose-response curves for cell viability of A549 cells treated with different formulations were depicted, and the IC50 was calculated using GraphPad Prism (Version 6.01).

4.4 Results

4.4.1 Fluorescence Imaging of A549 Cells after Exposure to Formulations for 3 h

The A549 cells in 6-well plates were treated with formulations at 14.69 μM CytC, 0.685 mM total lipids, and 0.294 mM phosphate from MgP for 3 hours and the results of the following florescent imaging are presented in Fig. 4 and Table 4.1.

Cells treated with free Alexa 488-labeled CytC did not display significant green fluorescence (Fig. 4.1. (A) and Table 4.1.), indicating that Alexa 488-labeled CytC could not efficiently penetrate through cell membrane into the A549 cells. Furthermore, CytC LP/MgP caused much more cargo protein CytC attached to A549 cells than any other formulations and the no-treatment group as indicated by the strongest green fluorescence of the corresponding cells (Fig. 4.1. (B) and Table 4.1.).

CytC LP/MgP and bare LP displayed less mitochondrial staining than other formulations and the no-treatment group, (Fig. 4.2. (B), (C), (D) and Table 4.1.). In addition, CytC LP/MgP and bare LP displayed more nuclear staining than other formulations and the no-treatment group, (Fig. 4.3. (B), (C), (D) and Table 4.1.).

A B

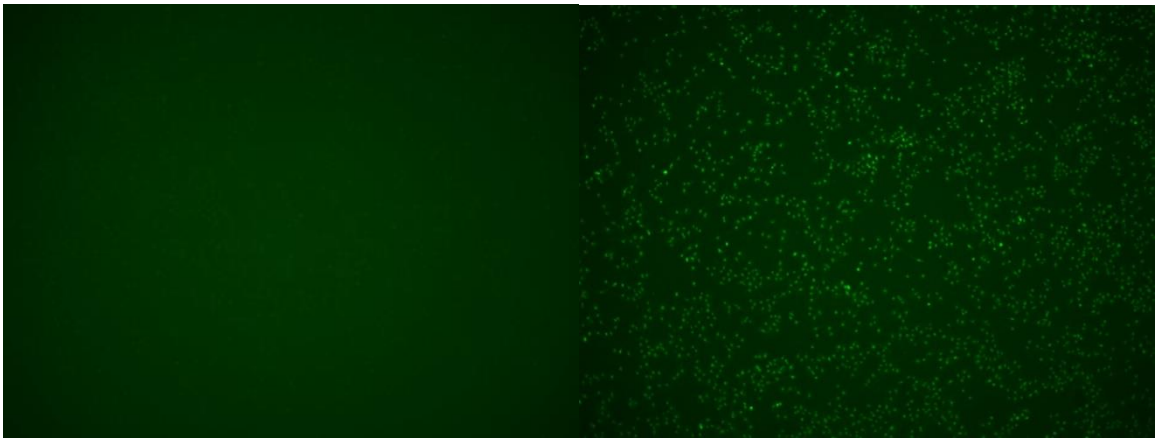

C D

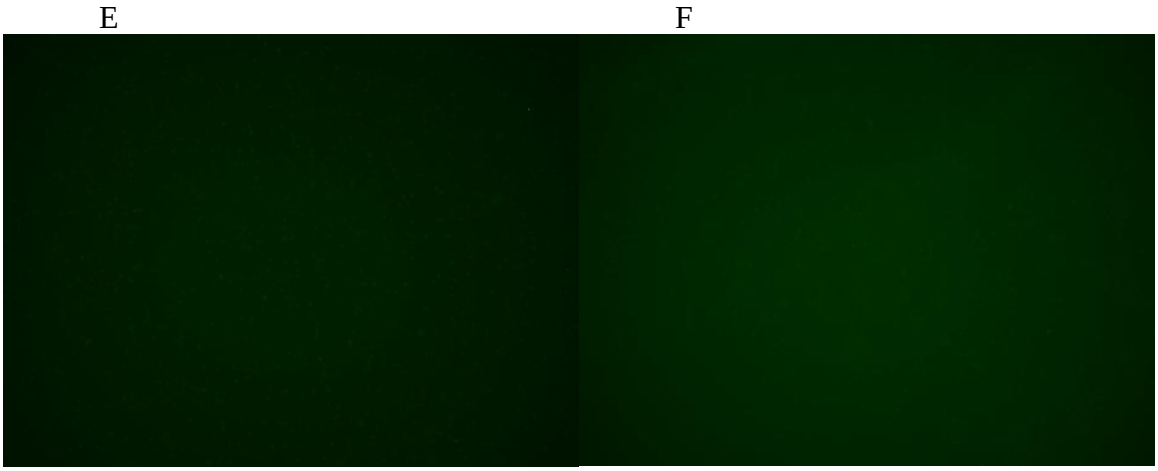

Fig. 4.1. The attachment of Alexa 488-labeled cytochrome c to A549 cells after 3 h incubation with (A)Alexa 488-labeled CytC, (B)Alexa 488-labeled CytC LP/MgP, (C)bare LP/MgP, (D)bare LP, (E)Alexa 488-labeled CytC+MgP, and (F)no-treatment group measured as shown by fluorescence microscopy.

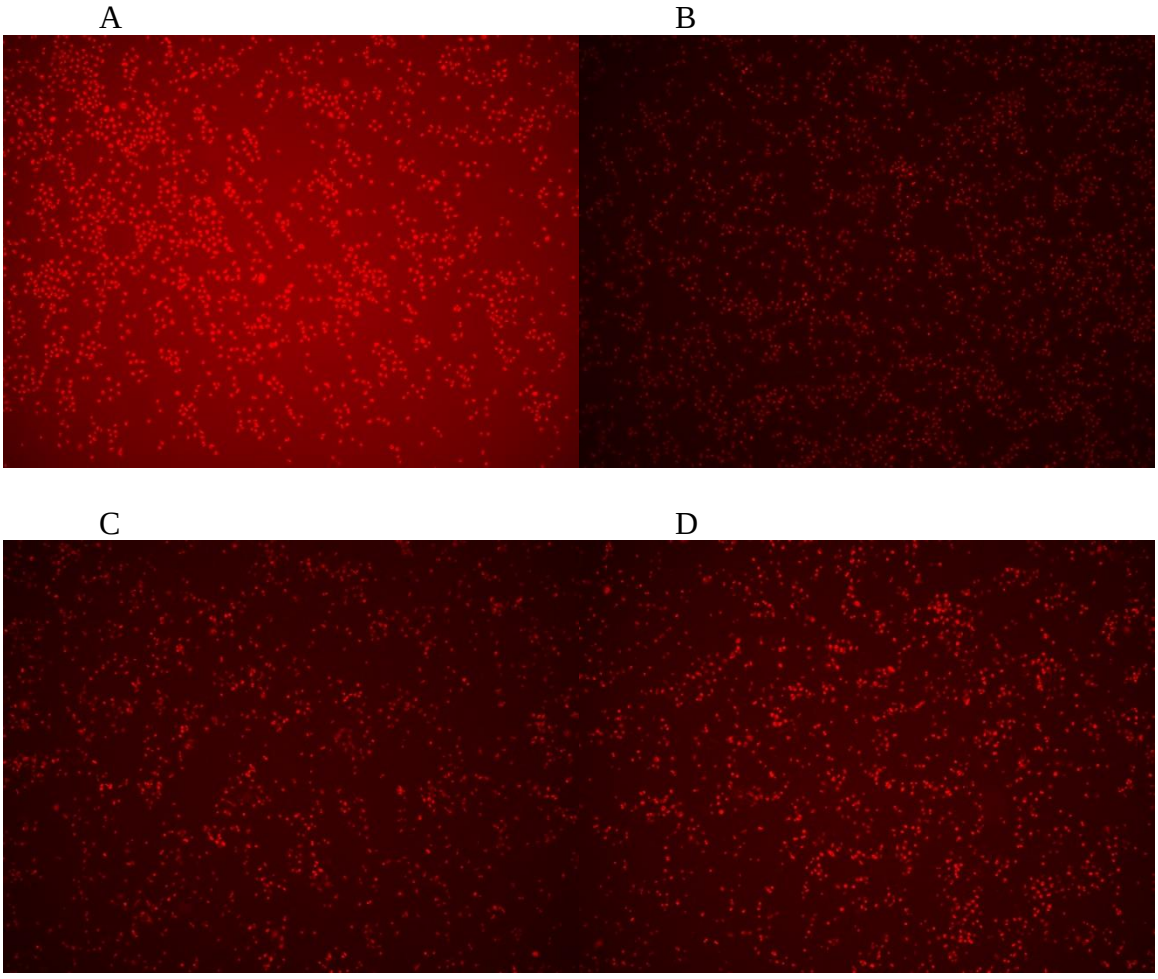

E F

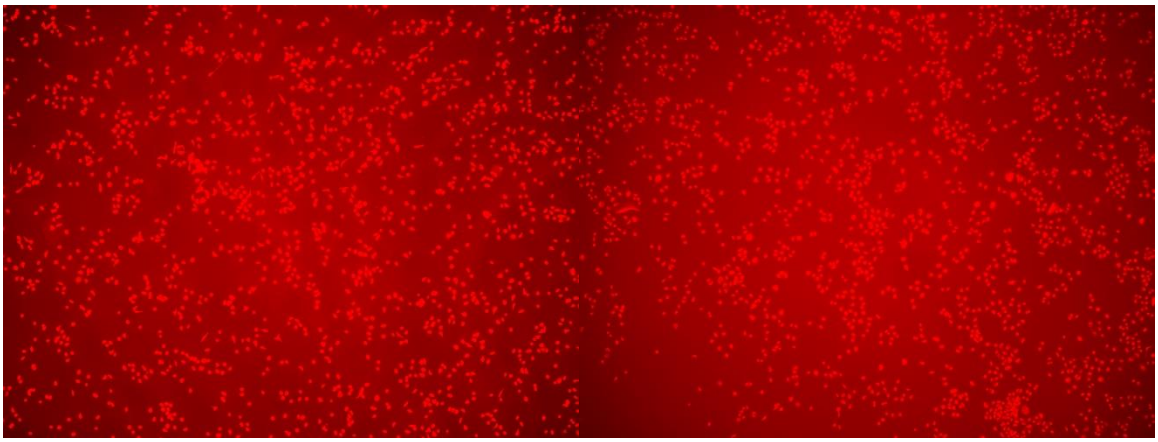

Fig. 4.2. The uptake and intramitochondrial accumulation of MitoRed in A549 cells after 3 h incubation with (A)Alexa 488-labeled CytC, (B)Alexa 488-labeled CytC LP/MgP, (C)bare LP/MgP, (D)bare LP, (E)Alexa 488-labeled CytC+MgP, and (F)no-treatment group measured as shown by fluorescence microscopy.

A B

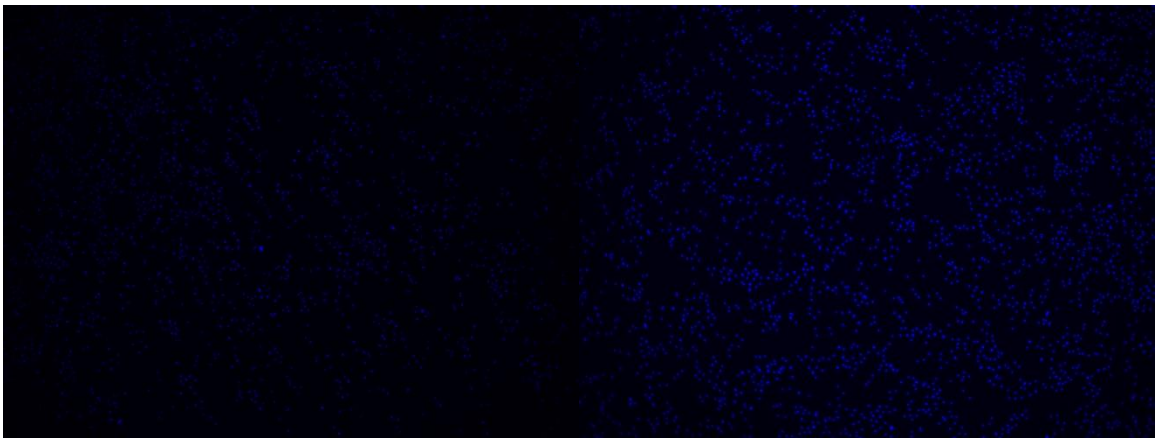

C D

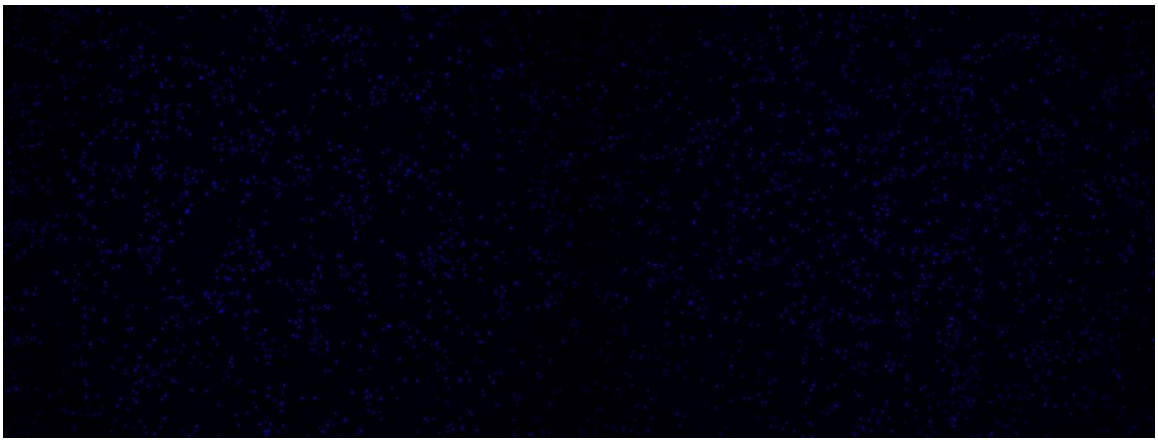

E F

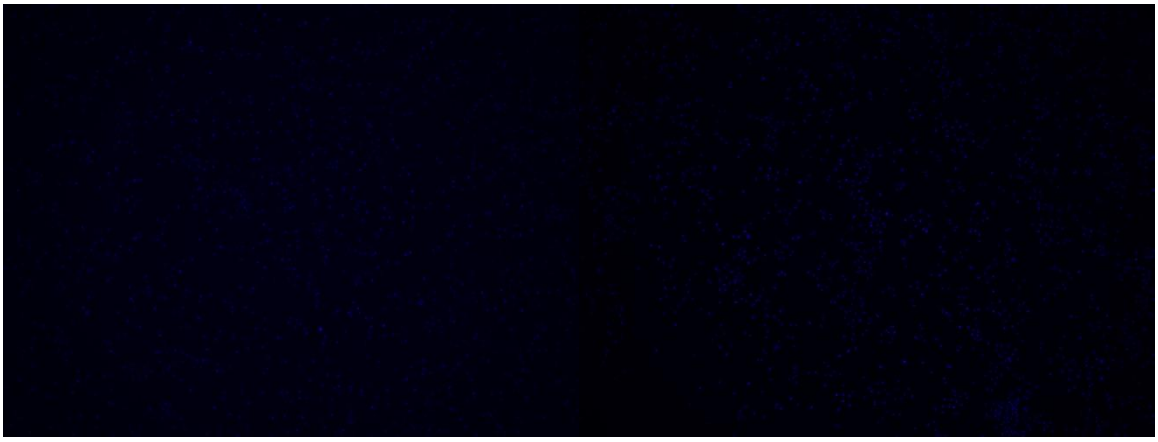

Fig. 4.3. The uptake and intranuclear accumulation of Hoechst 33342 in A549 cells after 3 h incubation with (A)Alexa 488-labeled CytC, (B)Alexa 488-labeled CytC LP/MgP, (C)bare LP/MgP, (D)bare LP, (E)Alexa 488-labeled CytC+MgP, and (F)no-treatment group measured as shown by fluorescence microscopy.

Table 4.1. Semi-quantitation of fluorescence intensity for staining of CytC, nuclei and mitochondria in A549 cells.

	CytC	**Nuclei**	**Mitochondria**
CytC	1±1	2511±34	25847±178
CytC LP/MgP	3616±42**	14305±114$^{\Delta\Delta}$	376±18$^{\#\#}$
CytC+MgP	2±1	1564±23	43399±238
Bare LP	1±1	5959±53$^{\Delta\Delta}$	5092±49$^{\#\#}$
Bare LP/MgP	1±1	6188±41$^{\Delta\Delta}$	1440±27$^{\#\#}$
No treatment	1±1	2868±36	41564±203

Each value represents the mean±S.D. of at least three measurements. Significant difference **P<0.01 *vs.* CytC of no treatment, $^{\Delta\Delta}$P<0.01 *vs.* nuclei of no treatment, and $^{\#\#}$P<0.01 *vs.* mitochondria of no treatment (Student's *t*-test).

4.4.2 MTS Assay on A549 Cell Viability after Exposure to Formulations for 48 h

The highest concentration of total lipids in wells of 96-well plates is 0.428 mM, and of phosphate from MgP is 0.184 mM. Free CytC showed relatively high cytotoxicity at low concentrations. At the same time, high cytotoxicity was observed in a concentration-dependent manner for bare LP with or without MgP. However, lower cytotoxicity was found from CytC LP/MgP than from bare LP with or without MgP.

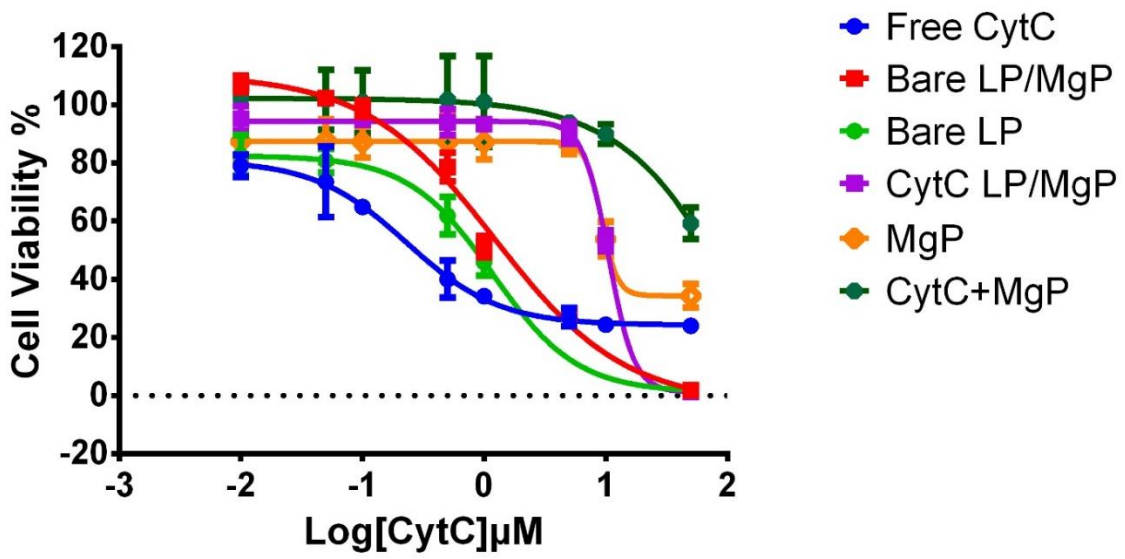

Fig. 4.4. MTS assay on cell viability after exposing A549 Cells to free CytC (blue), CytC LP/MgP (purple), bare LP/MgP (red), bare LP (green), CytC+MgP (dark green), and MgP (orange) for 48 h.

Table 4.2. IC50 normalized by the concentration of CytC.

	Free CytC	Bare LP/MgP	Bare LP	CytC LP/MgP	CytC LP	MgP	CytC+MgP
IC50 of CytC (µM)	~ 0.231	1.23	1.179	10.59	14.98	~ 9.21	~ 243.1

4.5 Discussion

4.5.1 Fluorescence Imaging

Sephadex® G-50 Fine gel filtration resin (GE Healthcare Life Sciences, Pittsburgh, PA) for the separation of molecules from 1,000 to 30,000 Dalton was used first to separate the conjugate from unreacted labeling reagent. However, the CytC (labeled or unlabeled) was poorly resolved from unreacted Alexa 488 dye on a 25 cm column, as indicated by Fig. 4.5, suggesting that CytC and unreacted Alexa 488 dye were

collected as a mixture. The poor resolution may be partly due to the small molecular weight of CytC (12 kDa).

Fig. 4.5. Column chromatography by Sephadex® G-50 Fine.

Sephadex® G-25 Medium gel filtration resin (GE Healthcare Life Sciences, Pittsburgh, PA) with a separation range of 1000 to 5000 Dalton was then attempted to improve the resolution. However, the CytC (labeled or unlabeled) was poorly resolved from unreacted Alexa 488 dye by a 25-cm column, as indicated by lack of two separate peaks of Alexa 488-labeled CytC and unreacted Alexa 488 dye by UV-Visible

Spectrometry readout at 488 nm (Fig. 4.6., the signal at 550 nm is from CytC), which meant CytC and unreacted Alexa 488 dye were collected simultaneous as a mixture.

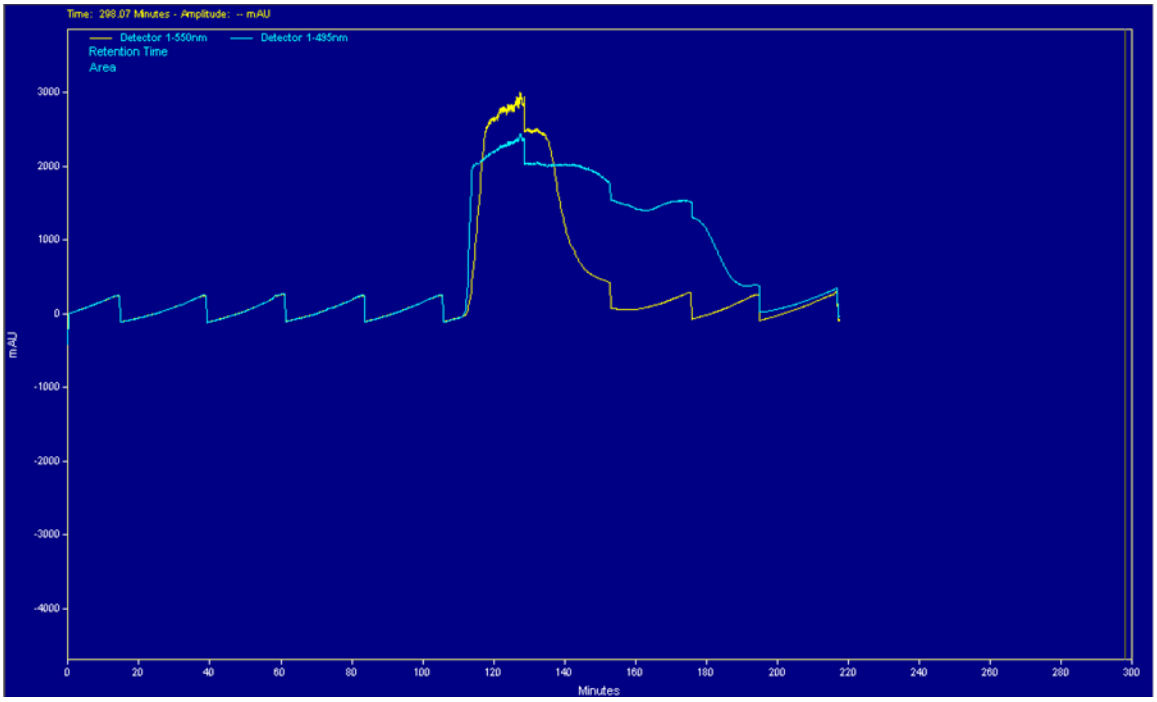

Fig. 4.6. UV-Visible Spectrometry readout for the separation of (yellow) CytC at 550 nm from (blue) Alexa 488 dye at 488 nm by Sephadex® G-25 Medium.

Eventually, Amicon® Ultra 15 mL centrifugal filter (EMD Millipore, Billerica, MA) with 3 kDa molecular weight cutoff allowed the separation of cytochrome c from the unreacted dye molecules whose molecular weight is smaller than 3 kDa. The protein-dye mixture was centrifuged twice on Centrifuge 5810 R (Eppendorf, Germany) at 4000 x g at 25 ℃ (1 h each time) to yield the labeled cytochrome c at a recovery rate of ~60%.

Jones *et al.* reported that CytC contains cell penetrating peptide (CPP) epitopes in the N- and C-terminal helices. Such CPPs can mediate the cellular uptake of free CytC protein [26]. The reason why Alexa 488-labeled CytC could not distribute into cells

might be that after NHS esters (or succinimidyl esters) of Alexa Fluor® 488 reacted with non-protonated aliphatic amine groups of proteins to form stable carboxamide bonds, the conjugated Alexa 488 moiety hindered the cell penetrating peptide (CPP) epitopes in the N-terminal helices of CytC.

All formulations containing the cationic lipid DOTAP reduced the uptake and intramitochondrial accumulation of MitoRed, which is probably due to the change of mitochondria's inner transmembrane potential ($\Delta\Psi_m$) by DOTAP based on prior reports of mitochondrial staining. Petit *et al.* reported that the uptake of the fluorochrome Rhodamine 123 into mitochondria was reduced in pre-apoptotic cells [27]. The authors found that the fluorophore accumulated into the mitochondrial membrane matrix space in inverse proportion to $\Delta\Psi_m$ in a Nernst fashion, and thus proposed that the reduced dye uptake was due to the $\Delta\Psi_m$ dissipation. Moreover, Perry *et al.* reported that depolarization of $\Delta\Psi_m$ caused lower concentration of Rhodamine 123 in mitochondria, and *vice versa.* [28]. MitoRed is a cell membrane permeable Rhodamine-based dye that localizes in mitochondria and emits red fluorescence. The interaction of MitoRed with mitochondria depends on the membrane potential of mitochondria. Thus, the reduced mitochondrial staining of MitoRed strongly suggests that DOTAP in the proposed formulation of our project causes pre-apoptosis of A549 by dissipating the mitochondria's inner transmembrane potential.

All formulations containing cationic lipid DOTAP increased the uptake and intranuclear accumulation of Hoechst 33342. Faleiro *et al.* found that caspase-9, which is activated earlier than caspase-3, directly or indirectly increases permeability of nuclear pores. This increment allows caspase-3 and other molecules that could not pass through

nuclear pores in living cells to enter or leave the nucleus during apoptosis by diffusion [29]. Therefore, the increased nuclear staining by Hoechst 33342 in cells treated with formulations with DOTAP again attests DOTAP's apoptotic effect on the A549 cells.

It is not totally clear whether Alexa 488-labeled CytC is outside or inside of A549 cells. This can be resolved as future work by using confocal microscopy with higher magnification. In addition, membrane impermeable fluorescent quenchers can be applied to the outside of such cells to test whether the fluorescence of Alexa 488-labeled CytC can be changed: a reduction of the fluorescence would indicate the formulation is still on the cell surface and vice versa.

4.5.2 Cell Viability Assay

Our data showed that free CytC caused the strong cytotoxicity, which is intriguing in the context of prior reports on CytC's effects on cell viability. Among earlier investigations, Piel *et al.* found that after intravenous injection in a septic mice model, bovine heart CytC was taken up by cardiomyocytes and significantly improved cardiomyocytes' mitochondrial function. Further, the survival rate of the cardiomyocytes increased from 15% to about 50% in the septic mice that received CytC injections [20], [21]. These findings may seem puzzling because CytC not only has to be taken up by cells, but also must translocate across the cell membrane to accumulate in mitochondria. This is now better explained by Jones *et al*, who showed that CytC contains cell penetrating peptide (CPP) epitopes in the N- and C-terminal helices [26]. Such CPPs can mediate the cellular uptake of various proteins. Therefore, cytotoxicity of free Alexa 488-labeled CytC needs to be evaluated in the future to validate whether the conjugated Alexa 488 moiety hindered CPPs in the N-terminal helices of CytC.

Nevertheless, another question needs to be addressed: why does the treatment with exogenous CytC, which will be taken up into the cytosol first, not amplify the apoptotic cascade but instead lead to increased survival of the cardiomyocytes in septic mice? This phenomenon conforms with our data that lower cytotoxicity was found from CytC LP/MgP than from bare LP with or without MgP. There were three likely interpretations. First, cationic lipid DOTAP changes mitochondrial membrane potential, generates reactive oxygen species (ROS), dissociates CytC from the inner mitochondrial membrane, forms the mitochondrial outer membrane permeabilization pore (MOMPP), releases CytC from mitochondria, and induces apoptosis in different cell lines, all of which confirmed by Aramaki *et al.* [15]. The release of endogenous CytC, which is an essential component of the electron transport chain (ETC leads to mitochondrial dysfunction. It has long been known that isolated mitochondria can reversibly release and take up CytC, while the latter restores mitochondrial function, as demonstrated by Jacobs and Sanadi [19], Doran and Halestrap [32]. Thus, exogenous CytC delivered by CytC LP/MgP in the cytosol could enter mitochondria to restore ETC activity of mitochondria and thus increase the cell viability. This explanation was supported by the aforementioned studies of an animal model for sepsis [20], [21].

As the second interpretation, Zhivotovsky *et al.* and Li *et al.* reported that CytC-induced apoptosis is dependent on the concentration of the cytosolic CytC [30], [31]. Clayton *et al.* explained that endogenous CytC release occurs proportionally to the extent of cellular ‘stress’, and each cell, even from the same cell line, responds to a certain threshold of the released CytC to progress into apoptosis [23]. Zhivotovsky *et al.* found that microinjected 10 μM or 20 μM CytC could induce apoptosis in various cell types,

and this effect was dependent on the cytosolic CytC concentration. Nevertheless, the apoptotic effect of 20 μM exogenous CytC was totally reversed when rat kidney (NRK) epithelial cells were transfected to express Bax/Bak, which are members of Bcl-2 family proteins known to induce formation of MOMPP (Fig. 4.7.) [30]. In this case, the exogenous CytC entered mitochondria through MOMPP by active transport [32], leading to a great decrement of cytosolic CytC concentration and protection of MOMPP-expressing cells from apoptosis. Cationic lipid DOTAP also leads to formation of the mitochondrial outer membrane permeabilization pore (MOMPP) [15]. Therefore, after the cells were exposed to CytC LP/MgP, DOTAP would induce MOMPP formation in the affected pre-apoptotic cells, followed by a translocation of the exogenous cargo protein CytC from the cytosol into the mitochondria. This would then protect the DOTAP-injured cells from entering apoptosis, resulting in higher cell viability.

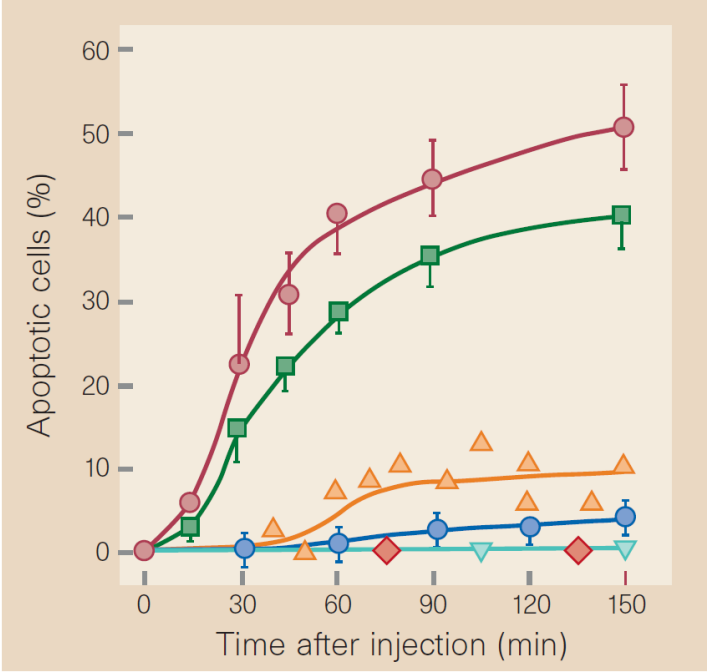

Fig. 4.7. Effect of CytC microinjection in normal rat kidney (NRK) epithelial cells. Wild-type cells were injected with 20 µM (dark red) or 10 µM (green) CytC. Cells expressing MOMPP were injected with 20 µM CytC (orange) [30].

As the third possible interpretation, free CytC also functions as a universal radical scavenger within the mitochondrial inner-membrane space. Because CytC constantly undergoes oxidation/reduction cycles in a respiring cell, it contributes to detoxification reactions against superoxide and hydrogen peroxide [22]. It is known that cationic lipid DOTAP enhances generation of reactive oxygen species (ROS), which eventually induces apoptosis [15]. Exogenous CytC delivered by CytC LP/MgP in the cytosol may act as a ROS scavenger like catalase, which removes DOTAP-generated ROS, and rescue cells from DOTAP-induced apoptosis.

Although the mechanism is still unclear, CytC decreases cytotoxicity of cationic lipids, which will facilitate the pharmaceutical applications of the latter in drug delivery systems.

4.6 Conclusion

CytC LP/MgP successfully led to the attachment of CytC to A549 cells. Intracellular delivery of CytC alleviated the cytotoxicity of cationic lipids in A549 cells, which could facilitate the clinical use of cationic lipids in drug delivery systems.

REFERENCES

[1]. Leader, Benjamin, Quentin J. Baca, and David E. Golan. "Protein therapeutics: a summary and pharmacological classification." *Nature reviews. Drug discovery* 7, no. 1 (2008): 21.

[2]. Moghimi, S. Moein, A. Christy Hunter, and J. Clifford Murray. "Long-circulating and target-specific nanoparticles: theory to practice." *Pharmacological reviews* 53, no. 2 (2001): 283-318.

[3]. Abarzúa, Patricio, Joseph E. LoSardo, Mary Lou Gubler, and Anthony Neri. "Microinjection of monoclonal antibody PAb421 into human SW480 colorectal carcinoma cells restores the transcription activation function to mutant p53." *Cancer Research* 55, no. 16 (1995): 3490-3494.

[4]. Marrero, Mario B., Bernhard Schieffer, William G. Paxton, Elisabeth Schieffer, and Kenneth E. Bernstein. "Electroporation of pp60c− src Antibodies Inhibits the Angiotensin II Activation of Phospholipase C-γ1 in Rat Aortic Smooth Muscle Cells." *Journal of Biological Chemistry* 270, no. 26 (1995): 15734-15738.

[5]. Slowing, Igor I., Brian G. Trewyn, and Victor S-Y. Lin. "Mesoporous silica nanoparticles for intracellular delivery of membrane-impermeable proteins." *Journal of the American Chemical Society* 129, no. 28 (2007): 8845-8849.

[6]. Räägel, Helin, Pille Säälik, Mats Hansen, Ülo Langel, and Margus Pooga. "CPP–protein constructs induce a population of non-acidic vesicles during trafficking through endo-lysosomal pathway." *Journal of Controlled Release* 139, no. 2 (2009): 108-117.

[7]. Zelphati, Olivier, Yan Wang, Shinichi Kitada, John C. Reed, Philip L. Felgner, and Jacques Corbeil. "Intracellular delivery of proteins with a new lipid-mediated delivery system." *Journal of Biological Chemistry* 276, no. 37 (2001): 35103-35110.

[8]. Kim, Sang Kyoon, Michael B. Foote, and Leaf Huang. "The targeted intracellular delivery of cytochrome C protein to tumors using lipid-apolipoprotein nanoparticles." *Biomaterials* 33, no. 15 (2012): 3959-3966.

[9]. Zuris, John A., David B. Thompson, Yilai Shu, John P. Guilinger, Jeffrey L. Bessen, Johnny H. Hu, Morgan L. Maeder, J. Keith Joung, Zheng-Yi Chen, and David R. Liu. "Efficient Delivery of Genome-Editing Proteins In Vitro and In Vivo." *Nature biotechnology* 33, no. 1 (2015): 73.

[10]. Naidu, Prathyusha. "Catalase-loaded liposomal magnesium phosphate nanoparticles for intracellular protein delivery." PhD diss., University of the Pacific, 2016.

[11]. Olton, Dana, Jinhua Li, Mary E. Wilson, Todd Rogers, John Close, Leaf Huang, Prashant N. Kumta, and Charles Sfeir. "Nanostructured calcium phosphates

(NanoCaPs) for non-viral gene delivery: influence of the synthesis parameters on transfection efficiency." *Biomaterials* 28, no. 6 (2007): 1267-1279.

[12]. Kawakami, Shigeru, Sachiko Suzuki, Fumiyoshi Yamashita, and Mitsuru Hashida. "Induction of apoptosis in A549 human lung cancer cells by all-trans retinoic acid incorporated in DOTAP/cholesterol liposomes." *Journal of controlled release* 110, no. 3 (2006): 514-521.

[13]. Lin, Paulo JC, Yuen Yi C. Tam, Ismail Hafez, Ammen Sandhu, Sam Chen, Marco A. Ciufolini, Ivan R. Nabi, and Pieter R. Cullis. "Influence of cationic lipid composition on uptake and intracellular processing of lipid nanoparticle formulations of siRNA." *Nanomedicine: Nanotechnology, Biology and Medicine* 9, no. 2 (2013): 233-246.

[14]. Wasungu, L. B. "Gene delivery with cationic lipids." (2006).

[15]. Aramaki, Yukihiko, Shuhei Takano, and Seishi Tsuchiya. "Cationic liposomes induce macrophage apoptosis through mitochondrial pathway." *Archives of biochemistry and biophysics* 392, no. 2 (2001): 245-250.

[16]. Roy, Indrajit, Susmita Mitra, Amarnath Maitra, and Subho Mozumdar. "Calcium phosphate nanoparticles as novel non-viral vectors for targeted gene delivery." *International Journal of Pharmaceutics* 250, no. 1 (2003): 25-33.

[17]. Li, Jun, Yun-Ching Chen, Yu-Cheng Tseng, Subho Mozumdar, and Leaf Huang. "Biodegradable calcium phosphate nanoparticle with lipid coating for systemic siRNA delivery." *Journal of controlled release* 142, no. 3 (2010): 416-421.

[18]. Tseng, Yu-Cheng, Angela Yang, and Leaf Huang. "How does the cell overcome LCP nanoparticle-induced calcium toxicity?." *Molecular pharmaceutics* 10, no. 11 (2013): 4391-4395.

[19]. Jacobs, Earl E., and D. R. Sanadi. "The reversible removal of cytochrome c from mitochondria." *Journal of Biological Chemistry* 235, no. 2 (1960): 531-534.

[20]. Piel, David A., Clifford S. Deutschman, and Richard J. Levy. "Exogenous cytochrome C restores myocardial cytochrome oxidase activity into the late phase of sepsis." *Shock (Augusta, Ga.)* 29, no. 5 (2008): 612.

[21]. Piel, David A., Peter J. Gruber, Carla J. Weinheimer, Michael R. Courtois, Charles M. Robertson, Craig M. Coopersmith, Clifford S. Deutschman, and Richard J. Levy. "Mitochondrial resuscitation with exogenous cytochrome c in the septic heart." *Mitochondrion* 6, no. 5 (2006): 2-3.

[22]. Hüttemann, Maik, Petr Pecina, Matthew Rainbolt, Thomas H. Sanderson, Valerian E. Kagan, Lobelia Samavati, Jeffrey W. Doan, and Icksoo Lee. "The multiple functions of cytochrome c and their regulation in life and death decisions of the mammalian cell: From respiration to apoptosis." *Mitochondrion* 11, no. 3 (2011): 369-381.

[23]. Clayton, Rebecca, John B. Clark, and Martyn Sharpe. "Cytochrome c release from rat brain mitochondria is proportional to the mitochondrial functional deficit: implications for apoptosis and neurodegenerative disease." *Journal of neurochemistry* 92, no. 4 (2005): 840-849.

[24]. Tamimi, Faleh, Damien Le Nihouannen, David C. Bassett, Suzette Ibasco, Uwe Gbureck, Jonathan Knowles, Adrian Wright, Andrew Flynn, Svetlana V. Komarova, and Jake E. Barralet. "Biocompatibility of magnesium phosphate

minerals and their stability under physiological conditions." *Acta biomaterialia* 7, no. 6 (2011): 2678-2685.

[25]. What Is Non-Small Cell Lung Cancer? [Internet]. Available from: https://www.cancer.org/cancer/non-small-cell-lung-cancer/about/what-is-non-small-cell-lung-cancer.html#references

[26]. Jones, Sarah, Tina Holm, Imre Mäger, Ülo Langel, and John Howl. "Characterization of bioactive cell penetrating peptides from human cytochrome c: protein mimicry and the development of a novel apoptogenic agent." *Chemistry & biology* 17, no. 7 (2010): 735-744.

[27]. Petit, Patrice Xavier, Naoufal Zamzami, Jean-Luc Vayssière, Bernard Mignotte, Guido Kroemer, and Maria Castedo. "Implication of mitochondria in apoptosis." In *Detection of Mitochondrial Diseases*, pp. 185-188. Springer US, 1997.

[28]. Perry, Seth W., John P. Norman, Justin Barbieri, Edward B. Brown, and Harris A. Gelbard. "Mitochondrial membrane potential probes and the proton gradient: a practical usage guide." *Biotechniques* 50, no. 2 (2011): 98.

[29]. Faleiro, Lavina, and Yuri Lazebnik. "Caspases disrupt the nuclear-cytoplasmic barrier." *J Cell Biol* 151, no. 5 (2000): 951-960.

[30]. Zhivotovsky, Boris, Sten Orrenius, Odd T. Brustugun, and Stein O. Døskeland. "Injected cytochrome c induces apoptosis." *Nature* 391, no. 6666 (1998): 449.

[31]. Li, Feng, Anu Srinivasan, Yu Wang, Robert C. Armstrong, Kevin J. Tomaselli, and Lawrence C. Fritz. "Cell-specific Induction of Apoptosis by Microinjection of Cytochrome c Bcl-xL HAS ACTIVITY INDEPENDENT OF CYTOCHROMEc RELEASE." *Journal of Biological Chemistry* 272, no. 48 (1997): 30299-30305.

[32]. DORAN, Elena, and Andrew P. HALESTRAP. "Cytochrome c release from isolated rat liver mitochondria can occur independently of outer-membrane rupture: possible role of contact sites." *Biochemical Journal* 348, no. 2 (2000): 343-350.